ENSO related variation of equatorial MRG and Rossby waves and forcing from higher latitudes

It is advisable to refer to the publisher's version if you intend to cite from the work. See Guidance on citing.

To link to this article DOI: http://dx.doi.org/10.1002/qj.2842

www.reading.ac.uk/centaur

RMetS

Royal Meteorological Society
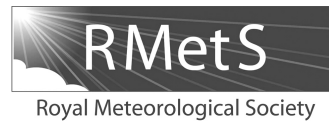
ENSO-related variation of equatorial MRG and Rossby waves and forcing from higher latitudes

Gui-Ying Yang[a,b]* and Brian J. Hoskins[b,c]

[a]*Climate Directorate, National Centre for Atmospheric Science, University of Reading, UK*
[b]*Department of Meteorology, University of Reading, UK*
[c]*Grantham Institute for Climate Change, Imperial College, London, UK*

Correspondence to: G.-Y. Yang, Department of Meteorology, University of Reading, Earley Gate, Reading RG6 6BB, UK. E-mail: g.y.yang@reading.ac.uk

The contrasting behaviour of westward-moving mixed Rossby–gravity (WMRG) and the first Rossby (R1) waves in El Niño (EN) and La Niña (LN) seasons is documented with a focus on the Northern Hemisphere winter. The eastward-moving variance in the upper troposphere is dominated by WMRG and R1 structures that appear to be Doppler-shifted by the flow and are referred to as WMRG-E and R1-E. In the east Pacific and Atlantic the years with stronger equatorial westerly winds, LN in the former and EN in the latter, have the stronger WMRG and WMRG-E. In the east Pacific, R1 is also a maximum in LN. However, R1-E exhibits an eastward shift between LN and EN.

The changes with El Niño/Southern Oscillation (ENSO) phase provide a test bed for the understanding of these waves. In the east Pacific and Atlantic, the stronger WMRG-E and WMRG with stronger westerlies are in accord with the dispersion relation with simple Doppler-shifting by the zonal flow. The possible existence of free waves can also explain stronger R1 in EN in the Eastern Hemisphere. 1-D free-wave propagation theory based on wave activity conservation is also important for R1. However, this theory is unable to explain the amplitude maxima for other waves observed in the strong equatorial westerly regions in the Western Hemisphere, and certainly not their ENSO-related variation. The forcing of equatorial waves by higher-latitude wave activity and its variation with ENSO phase is therefore examined. Propagation of extratropical eastward-moving Rossby wave activity through the westerly ducts into the equatorial region where it triggers WMRG-E is favoured in the stronger westerlies, in LN in the east Pacific and EN in the Atlantic. It is also found that WMRG is forced by Southern Hemisphere westward-moving wave trains arching into the equatorial region where they are reflected. The most significant mechanism for both R1 and R1-E appears to be lateral forcing by subtropical wave trains.

Key Words: equatorial waves; ENSO phase; westerly duct; lateral forcing; zonal propagation; equatorward propagation

Received 7 August 2015; Revised 10 May 2016; Accepted 19 May 2016; Published online in Wiley Online Library

1. Introduction

Equatorial waves and their associated tropical convection are fundamental components of the tropical climate system. Understanding the impact of El Niño/Southern Oscillation (ENSO) on equatorial waves is important for the improvement of weather forecasting in the Tropics and the extratropics on time-scales beyond a few days, and is also likely to be crucial for climate prediction (e.g. Lin *et al.*, 2006; Ringer *et al.*, 2006; Yang *et al.*, 2009). However, there have been few relevant observational studies, and theoretical understanding is limited. Yang and Hoskins (2013) have shown the sensitivity of equatorial Kelvin waves, in the domain of zonal wave-numbers 2–10 and

periods 2–30 days, and their associated convection over the central-eastern Pacific, to ENSO variations. El Niño (EN) events enhance, and La Niña (LN) events suppress the variability of upper tropospheric Kelvin waves and their associated convection, in both extended boreal winter and summer seasons.

One of the two major aims of this article is to document and examine the impact of ENSO on the behaviour of the other, rotationally dominated, gravest waves in this wave-number–frequency domain, the Westward Mixed Rossby–Gravity wave (WMRG) and the First Rossby (R1) wave.

A major context of this article is the understanding of the impact of zonal variations of the ambient flow on equatorial waves. A number of observational and theoretical studies have

shown that the ambient zonal flow significantly affects equatorial wave behaviour (e.g. Webster and Holton, 1982; Webster and Chang, 1988; Zhang, 1993; Tomas and Webster, 1994; Chang and Webster, 1995; Matthews and Kiladis, 1999; Hoskins and Yang, 2000; Yang *et al.*, 2007a, 2007b, 2007c, 2011, 2012; Yang and Hoskins, 2013; Dias and Kiladis, 2014). In Hoskins and Yang (2016, hereafter HY16) the theory for one-dimensional (1-D) propagation in a longitudinally varying zonal flow has been developed. It has then been applied, using the climatological upper tropospheric equatorial zonal wind, U, as the background flow, to examine to what extent 1-D equatorial propagation can explain the observed climatological distribution of the gravest equatorial waves. The theory gives that the energy and zonal wave number of Kelvin waves will vary in longitude in the opposite sense to U, with maxima occurring in minima in U. This accords well with the observed distribution of Kelvin waves. However, in HY16 the observed boreal winter distributions of the WMRG and R1 waves show maxima in the strong westerlies in the Western Hemisphere, which are not consistent with the dominance of 1-D equatorial propagation of free waves in the climatological flow.

The failure of this theory for WMRG and R1 waves in the Western Hemisphere focuses attention on the forcing of the waves there, and in particular the forcing from higher latitudes in the regions of upper tropospheric equatorial westerlies and the westerly ducts. This forcing can be expected to be sensitive to ENSO as both the westerly ducts and, as will be seen later, the subtropical wave activity, vary significantly with the phase of ENSO. The second aim of this article is, therefore, to examine and understand the higher-latitude forcing of WMRG and R1 waves in the Western Hemisphere through examination of the two phases of ENSO.

The present study will mainly consider the boreal winter period, November to April, which will be referred to as winter. As motivation, Figure 1(a) and (b) show the raw power spectra for winter 200 hPa, 15°S to 15°N averaged meridional winds for EN and LN phases in the Western Hemisphere, separated into those for the components of meridional wind that are symmetric and antisymmetric about the Equator. Shown are composites for seven EN and seven LN winters, which are defined below in section 2. The right panels show the EN − LN differences in power. Significant ENSO changes are seen in zonal wave-numbers 3−9 and periods longer than 5 days. The symmetric variance (Figure 1(a)) has larger wave activity in LN for both westward (negative wave number) and eastward-moving variance. The situation is less clear for the antisymmetric component (Figure 1(b)), though the westward component shows an LN maximum for a 10-day period and the eastward component shows generally slightly larger values in EN. Because of the interest in higher-latitude forcing, the power spectra of the variance in subtropical meridional wind in the two hemispheres are shown in Figure 1(c) and (d). The two hemispheres are similar to each other but with larger power in the Northern Hemisphere (NH). They are also similar to those for the deep Tropics, though with greater power (note the different scales). This raises the possibility that the power in the tropical region merely reflects an aliasing of the higher-latitude activity. However, it will be shown that this is not the case. The EN − LN differences are similar in the two hemispheres, there being more eastward activity in the band of interest in EN. Again, both hemispheres have a less clear message for the westward component, with LN being larger for a 10-day period.

Further motivation is provided in Figure 2 by the zonal and latitudinal variation of the mean zonal wind (Figure 2(a)) and the standard deviations of the eastward and westward components of the 200 hPa meridional wind, v, for winter (Figure 2(b) and (c)). In each case the full field composited for EN winters and for LN winters and their difference is given. Many features in this will be discussed below in section 5. Figure 2(a) shows that in EN winters, the NH subtropical jet is stronger and shifted southward, is more continuous and extends further east to around 300°E, consistent with that shown in Matthews and Kiladis (1999). In the Southern

Hemisphere (SH), the eastern Pacific subtropical westerlies are also stronger in EN. In contrast, the westerlies in 20°−30° belts in the Atlantic are stronger in LN winters. There is significant variation with ENSO in both eastward- and westward-moving variance. The strong eastward variance in the regions of the two westerly ducts (Figure 2(b)) is consistent with the equatorial westerly duct being favourable for extratropical wave activity propagating into the equatorial region and triggering equatorial waves, as proposed by Webster and Holton (1982) and shown in Yang *et al.* (2007c). It is notable that this is also the case for westward-moving activity, consistent with the modelling studies of Wang and Xie (1996) and Hoskins and Yang (2000) which show that WMRG and the R1 waves are stronger in a westerly region.

The eastward and westward variance in wave number and frequency bands like that seen as varying in Figure 1 will be considered to be predominantly associated with WMRG and R1 waves. This is consistent with Yang *et al.* (2007a, 2011, 2012), who found that in the zonal wave-number-frequency domain considered, gravity wave motions are not important and, surprisingly, as will be shown here in section 5, the largely rotational WMRG wave structure dominates over the east Pacific (hereafter E Pacific) and Atlantic not just for the westward symmetric variance of v but also for the eastward component. Similarly, the R1 structure dominates the eastward as well as the westward antisymmetric variance of v.

A summary of some of the equatorial wave theory that is the basis for the analysis technique and the data used will be given in section 2. Section 3 gives a summary of the theories associated with mechanisms that may influence the occurrence and nature of equatorial waves. These theories will be tested against observations of waves in the two ENSO phases. Section 4 will detail the observed variation of equatorial WMRG and R1 waves, and an analysis of the various mechanisms that may be important in giving the observed variation. Section 5 examines the importance of higher latitude forcing of equatorial waves. Section 6 contains a concluding discussion.
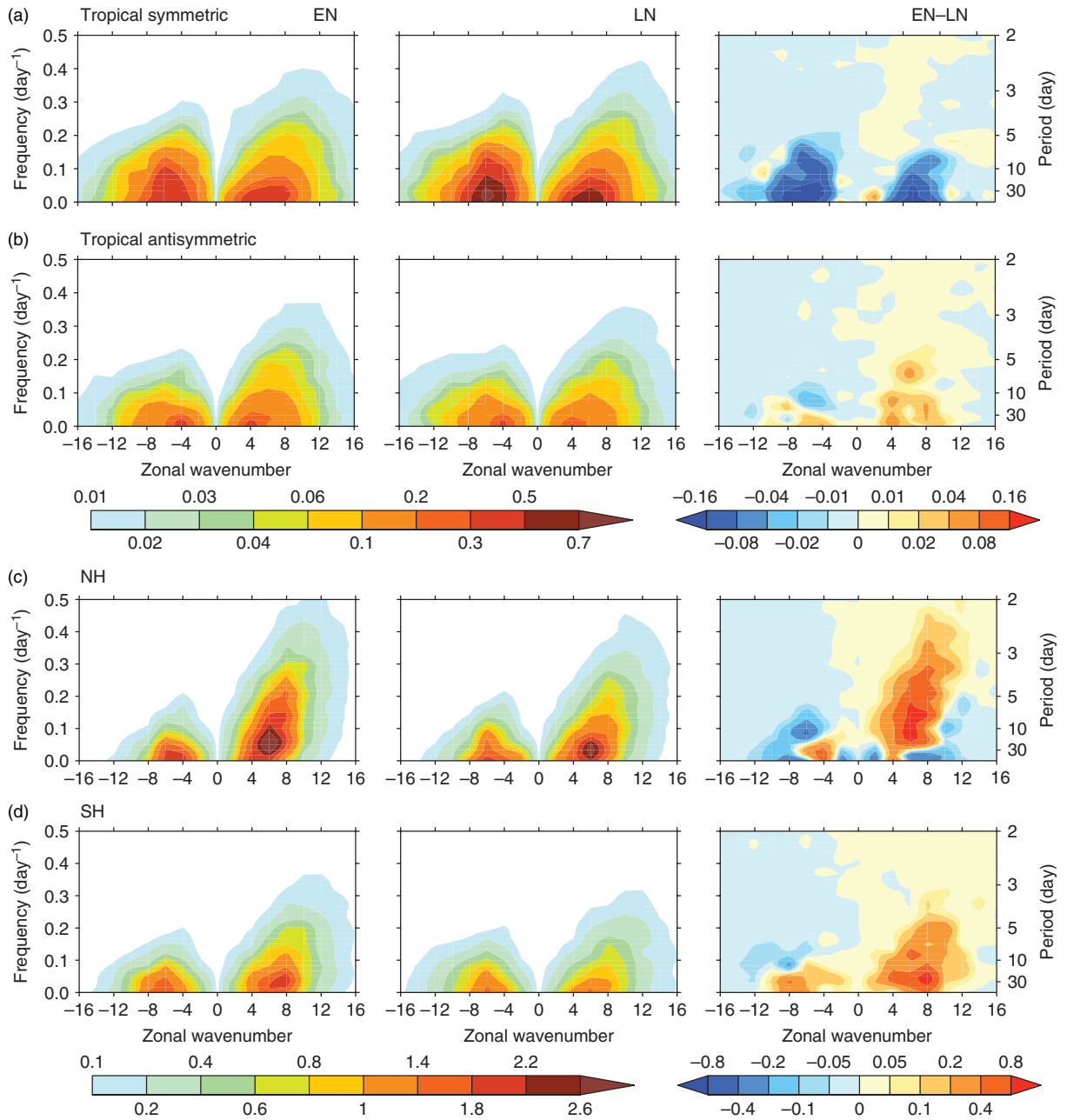
2. Methodology and data

Standard equatorial wave theory is based on linearization about an atmosphere at rest and separation of the vertical structure from that in the horizontal and time. Neglecting density variation for convenience, the equation for the vertical structure of the vertical velocity gives sinusoidal solutions provided zero vertical velocity boundary conditions are specified at the tropopause as well as at the ground. The separation constant may then be written $c^2 = \frac{N^2 H^2}{m^2 \pi^2}$ where m is the vertical mode number and H the height of the tropopause. For the first internal mode, $m = 1$, $c \approx 50 \, \mathrm{m \, s^{-1}}$. The horizontal equations are the shallow-water equations with gravity speed c, or 'equivalent depth', h, such that $gh = c^2$. Therefore, for the first internal mode, $h \approx 250 \, \mathrm{m}$. On an equatorial β-plane there is the Kelvin wave solution with zero v and $\omega = kc$, and there are solutions with non-zero v and the dispersion relation

$$\frac{\omega^2}{c\beta} - c\frac{k}{\omega} - \frac{c}{\beta}k^2 = (2n+1) \quad \text{for} \quad n = 0, 1 \ldots . \quad (1)$$

Since the Kelvin wave satisfies this relation with $n = -1$, then this notation is conventionally used to label it. The Kelvin wave is eastward moving. The MRG wave ($n = 0$) has both eastward- (EMRG) and westward-moving (WMRG) solutions. For $n = 1$ and higher modes there are westward-moving Rossby wave and both eastward- and westward-moving gravity wave solutions.

Although the separation of the vertical and horizontal structures is possible for a resting atmosphere, in general the separation of variables is not possible and analysis in terms of vertical modes and horizontal wave structures is not valid. Therefore in the methodology to separate equatorial waves, which was developed in Yang *et al.* (2003), no assumption about the

ⓒ 2016 The Authors. *Quarterly Journal of the Royal Meteorological Society* published by John Wiley & Sons Ltd on behalf of the Royal Meteorological Society.

Q. J. R. Meteorol. Soc. (2016)

Figure 1. Zonal wave-number-frequency power spectra of 200 hPa meridional wind, v, in the Western Hemisphere, in the Tropics (15°S to 15°N) for (a) component of v symmetric about the Equator, (b) component of v antisymmetric about the Equator, and (c) 20–30°N and (d) 20–30°S, for EN (left), LN (centre) winters and the difference (right) between composites at different phases of ENSO (EN − LN). Before performing the zonal Fourier analysis, the average in the 180° sector is removed and the values are taped to zero in the 18° regions at each end of the sector.

vertical structure or dispersion relation is made, but at each level the fields in the Tropics are projected onto the parabolic cylinder functions that describe the horizontal structures of theoretical equatorial waves. Some horizontal equatorial wave structures are shown in, for example, Yang *et al.* (2003).

As in Gill (1980), using variables,

$$q = u + gZ/c, \ r = u\text{-}gZ/c, \ v, \quad (2)$$

where (u, v) are horizontal winds and Z is geopotential height, wave solutions are found in terms of parabolic cylinder functions,

$$D_r\left(\frac{y}{y_0}\right) = \exp\left\{-\frac{1}{4}\left(\frac{y}{y_0}\right)^2\right\} P_r\left(\frac{y}{\sqrt{2}y_0}\right), \quad (3)$$

where

$$y_0 = \left(\frac{c}{2\beta}\right)^{1/2}. \quad (4)$$

P_r is proportional to a Hermite polynomial of order r, and the waves are trapped at the Equator on a scale $y_t = \sqrt{2}y_0$. The meridional scale y_0 is determined from a best fit to the data to be about 6° and it is found that the analysis is not sensitive to the particular value of y_0 chosen (Yang *et al.*, 2003, 2012).

Any flow can be projected onto the parabolic cylinder functions:

$$\{q, v, r\} = \sum_{n=0}^{n=\infty} \{q_n, v_n, \ r_n\} D_n. \quad (5)$$

These functions forms a complete and orthogonal basis, and the projections in Eq. (5) are quite general, with q_0D_0 describing the Kelvin wave, q_1D_1 and v_0D_0 describing the $n = 0$ MRG wave, and $q_{n+1}D_{n+1}$, v_nD_n and $r_{n-1}D_{n-1}$ describing $n \geq 1$ Rossby waves or gravity waves. Without assuming the vertical structure, this level-by-level projection technique was introduced in Yang *et al.* (2003) and has been successfully employed in a number of subsequent articles (Yang *et al.*, 2007a, 2007b, 2007c, 2011, 2012; Yang and Hoskins, 2013).
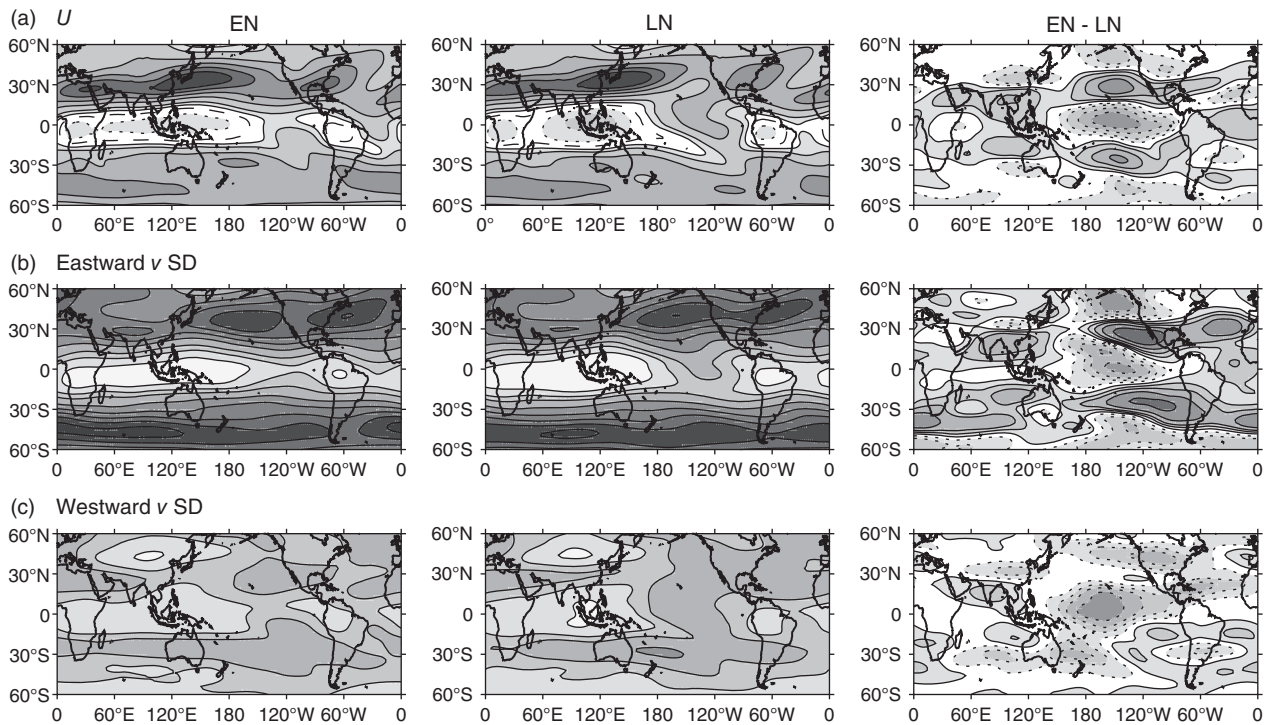
Figure 2. Average zonal winds (U) and perturbation meridional wind (v) amplitudes at 200 hPa for EN winter composites (left), LN winter composites (centre) and for their difference, EN − LN (right). (a) Zonal wind, (b) eastward v standard deviation (SD), and (c) westward v standard deviation. The units throughout are m s^{-1}, positive contours are continuous, negative contours dotted and the zero contour in the full field is dashed. Shading is used for values beyond the first positive or negative contour. In (a) the contours in the full fields are at 0, ±5, ±10, ±20 and then every 10, but at ±2, ±5, ±10 and then every 5 in the difference field with the zero contour suppressed. In (b) and (c) the contours for the full field are 1, 1.5, 2 then every 1, and the contour interval in the difference field is 0.2 with the lowest contours at ±0.1.

Data used in this study are 6-hourly u, v and Z from the European Centre for Medium-range Weather Forecasts (ECMWF) ERA-Interim re-analysis for the period from 1979 to 2010, with a horizontal resolution of about $0.7°$ and at 37 pressure levels from 1000 to 1 hPa. Detailed information on the data can be found in Dee *et al.* (2011). The three variables q, v and r between 20°N and 20°S at each level are separately projected onto parabolic cylinder functions as in Eq. (5). The projected $n = 0$ and $n = 1$ components will be referred to as WMRG and R1 waves. WMRG and R1 waves are found moving to the eastward due to Doppler shifting (HY16) as well as the westward direction so the former are referred to as WMRG-E and R1-E, respectively. The focus in this article is often on the meridional wind, v, and for this variable the individual wave contributions are orthogonal, and sum up to give the entire field.

As in our previous studies (Yang *et al.*, 2003, 2007a, 2007b, 2007c, 2011, 2012), before projection, the dynamical fields are first separated into eastward- and westward-moving components using a space–time spectral analysis. In order to focus on the spectral domain with most equatorial wave power, the data are filtered in a domain of zonal wave-number k from ±2 to ±10 and period from 2 to 30 days. It should be noted that this spectral domain is very broad compared with that used in most equatorial wave studies. The westward-moving component is used to analyse WMRG and R1 waves and the eastward-moving component is used to analyse the WMRG-E and R1-E waves.

Linear regression techniques similar to those used in Yang *et al.* (2007a, 2007b) are used in section 5 to examine extratropical forcing and the composite horizontal structures associated with equatorial waves. More details of the technique were given in Yang *et al.* (2007a, 2007b).

As in Yang and Hoskins (2013) due to the large seasonal variability of equatorial waves, for the analysis here the year is split into two 6-month periods, an extended boreal winter (November to April) and summer (May to October). These are referred to as 'winter' and 'summer'. Because the extratropical forcing for equatorial waves is more significant in winter, the analysis in this article will focus on this season, with the summer behaviour briefly mentioned in the final discussion.

In Yang and Hoskins (2013), EN/LN winters and summers were identified using the Niño-3.4 index and monthly Southern Oscillation Index (SOI) and these will be used here. There are seven EN winters (1982/1983, 1986/1987, 1991/1992, 1994/1995, 1997/1998, 2002/2003 and 2009/2010), seven LN winters (1988/1989, 1998/1999, 1999/2000, 2000/2001, 2005/2006, 2007/2008 and 2008/2009), five EN summers (1982, 1987, 1991, 1997 and 2002) and six LN summers (1988, 1989, 1998, 1999, 2000 and 2010). The results for composite EN and LN seasons are obtained by first calculating relevant quantities for each individual EN and LN season and then averaging the results for all EN or LN seasons, respectively.

3. Some theoretical considerations

This section gives a succinct review of the theories associated with mechanisms that may influence the occurrence and behaviour of equatorial waves.

3.1. Free equatorial waves

No assumption is made in the analysis technique used that the dispersion relation for resting atmosphere equatorial waves, Eq. (1), is valid. However, it is helpful to consider the impact on the dispersion relation of assuming that simple Doppler shifting by a uniform flow is both valid and relevant. This is illustrated in Figure 3 for the WMRG, and the R1 waves for an equivalent depth of 200 m, a large value which, especially for R1 waves, is chosen because it is more appropriate for the deeper vertical structure waves in the E Pacific (e.g. Yang *et al.*, 2007a, 2011, 2012) than the usual 40 m depth. For a resting atmosphere, the smaller depth is relevant to the gravest baroclinic structure in the vertical, and is likely to be more appropriate for the Eastern Hemisphere. The domain of interest in wave-number-frequency space in this article is indicated here by hatching. Vertical hatching indicates westward-moving waves and horizontal hatching eastward-moving waves.
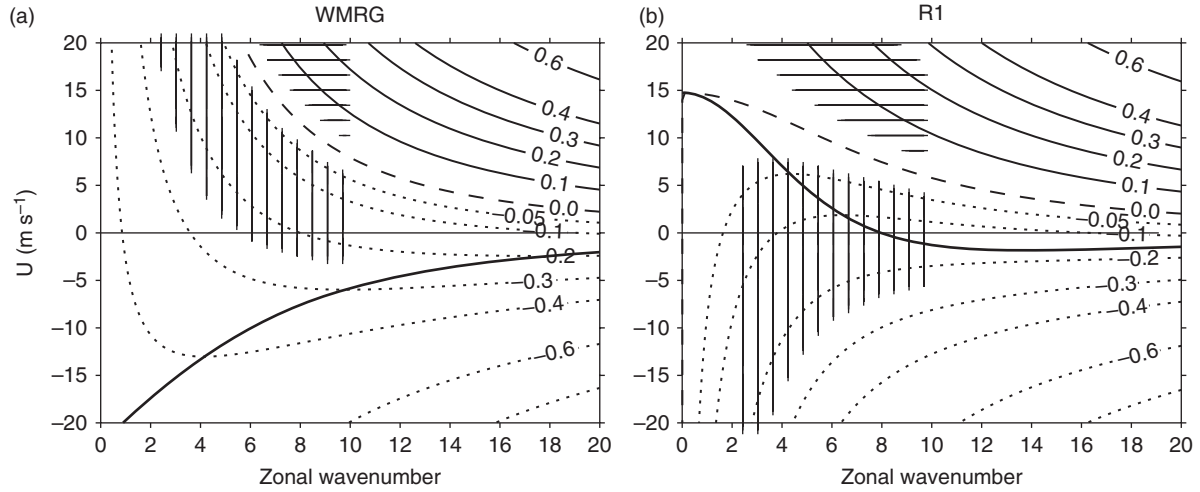
Figure 3. Doppler-shifted frequencies as a function of zonal wave number and ambient zonal wind for (a) WMRG and (b) R1 for an equivalent depth of 200 m ($c = 45\,\mathrm{m\,s}^{-1}$). The frequencies are given in cycles per day, with contours at 0, -0.05, ±0.1, ±0.2, etc. with the positive contours continuous, the zero contour dashed and negative contours dotted. The hatching indicates the region with zonal wave numbers and frequencies in the band of interest (k from 2 to 10 and period from 4 to 30 days), horizontal hatching for eastward-moving (WMRG-E and R1-E) and vertical hatching for westward-moving waves (WMRG and R1). The heavy solid line in each panel indicates $c_{gx} = 0$ (zero slope W of the frequency contour), with eastward group velocity in the region above and westward group velocity in the region below.

The WMRG wave can have eastward phase propagation in a sufficiently strong westerly flow. As mentioned above, such waves will be labelled WMRG-E, while WMRG will be used for the westward-moving wave. It should be noted that the WMRG-E structure is very different from the gravity-wave-like eastward-moving MRG (EMRG) wave structure for a resting atmosphere, as shown in e.g. Yang *et al.* (2003). The EMRG is found to be very weak in the band of interest. Similarly the R1 wave can have eastwards phase propagation as well as westwards and when moving eastwards will be denoted R1-E. The group velocity of WMRG and WMRG-E waves is eastwards (above the heavy solid line) in the band of interest. In contrast, R1 has a smaller group velocity relative to the flow and with the addition of the basic flow its wave activity can propagate eastwards or westwards. However, R1-E activity always propagates eastwards in the strong westerly flow. The picture is not very sensitive to the specification of the equivalent depth. For a 40 m depth (see Fig. 4 in HY16), WMRG-E waves are found in a larger range of wave numbers for westerly flow, with WMRG waves restricted to the lowest wave numbers. Also, in weak easterly flow, more low-wave-number WMRG waves are possible. R1 and R1-E free-wave activity is affected in a similar way.

The activity of equatorial waves has its largest amplitudes confined to the upper troposphere and there is interest in understanding how the large variations in the zonal flow in this region may influence the zonal propagation of wave activity. Consequently, in HY16 the theory of 1-D propagation on a varying zonal flow was developed and applied to equatorial waves. Following Lighthill (1978), a theoretical analysis in HY16 shows that for steady-state distribution of a particular wave, along a ray path, the longitudinal variation of its zonal wave number k is

$$\frac{dlnk}{dx} = -\frac{1}{c_g}\frac{dU}{dx}, \qquad (6)$$

where c_g is the group velocity and U is the basic zonal flow. Equation (6) indicates that along a ray path, k always has a tendency that is the opposite to that of U when c_g is positive, and the same as U when c_g is negative. The variation along a ray path of wave energy, E, is implied by the conservation equation for wave action density (e.g. Bretherton and Garrett, 1968; Lighthill, 1978). The theory developed in HY 16 shows that in a steady state, the zonal variation of E along a ray path is given by:

$$\frac{dlnE}{dx} = -\frac{B}{c_g}\frac{dU}{dx}. \qquad (7)$$

Here B is a property of the wave in question:

$$B = 1 + \frac{c_{gi}}{c_i} - \frac{k}{c_g}\frac{\partial c_{gi}}{\partial k}, \qquad (8)$$

where c_i is the intrinsic phase speed and c_{gi} the intrinsic group velocity (i.e. in a resting atmosphere). Values of B and B/c_g for each equatorial wave as a function of k and U have been presented in HY16. Equations (6) and (7) indicate that when B is positive, E behaves in a similar manner to k. Where c_g tends to zero, both E and k tend to infinity in the absence of dissipative processes: this is the wave accumulation of Chang and Webster (1995). However for B negative, E and k behave in opposite senses, with E having finite maxima at maxima in the flow for c_g positive and at minima in the flow for c_g negative.

For Kelvin waves which are non-dispersive, $B = 2$ and, assuming Doppler shifting by typical tropospheric zonal winds, c_g is always positive. The theory then gives that Kelvin wave E and k will both vary in longitude in the opposite sense to U, with maxima at minima in U. This accords well with the observed distribution of Kelvin waves as shown in HY16 and their ENSO-related variation shown in Yang and Hoskins (2013).

To aid in the understanding of the results from 1-D propagation theory for WMRG and R1 waves, Figure 4(a)–(c), taken from YH16, give some results of 30-day ray tracing of the wave energy for WMRG/WMRG-E with a period of 3 and 10 days (Figure 4(b)) and R1/R1-E with a period of 5 and 10 days (Figure 4(c)) waves for the smoothed winter climatological upper tropospheric flow shown in Figure 4(a). High frequency, short wavelength WMRG waves that can occur in the Eastern Hemisphere have B and c_g negative which, according to Eq. (7), implies that their E should have the opposite behaviour to the flow, having its maximum in the strongest easterlies, and decreasing into weaker easterlies as in Figure 4(b) ($30°-120°$ sector). In the westerlies in the Western Hemisphere both WMRG and WMRG-E waves are possible. Both have B and c_g positive. Therefore E and k for these waves behave in the opposite manner from the flow, having minima in westerly maxima and accumulating where c_g tends to zero, as in Figure 4(b) ($210°-360°$ sector). R1 waves exist in the Eastern Hemisphere easterlies and have B positive and c_g negative. Their E and k therefore mimic the flow with maxima in minimum easterlies and accumulation where c_g tends to zero, as in Figure 4(c) ($0°-150°$ sector). In the Western Hemisphere, R1 waves cannot exist for either period. However, analysis indicates that in the Western Hemisphere R1 waves can exist for lower frequency and larger h, consistent with the barotropic structure for the wave.
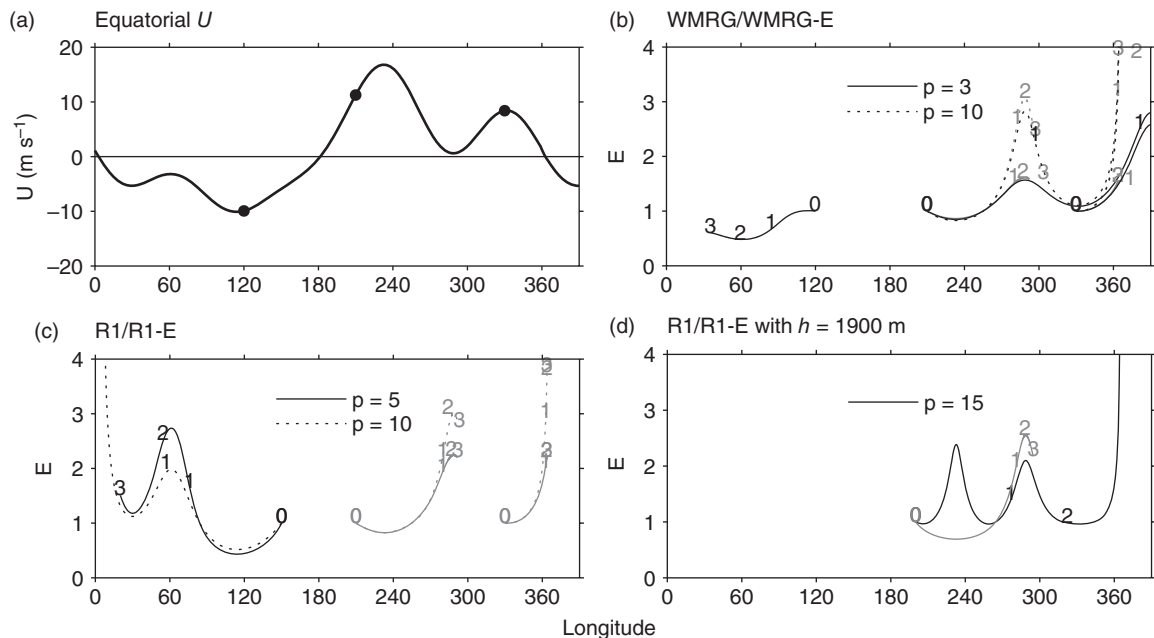
Figure 4. Ray tracing for WMRG and R1 waves on a smoothed upper-tropospheric winter zonal flow. (a) Zonal flow, (b) wave energy, E, for WMRG and WMRG-E waves, (c) wave energy, E, for R1 and R1-E waves. In (b), the starting points for the rays are 120°, 210° and 330°E, and the periods 3 days (solid) and 10 days (dotted). In (c), the starting points for the rays are 150°, 210° and 330°E, and the periods 5 days (solid) and 10 days (dotted). In (b) and (c), for rays starting in the Eastern Hemisphere, $h = 40$ m throughout. For rays starting in the Western Hemisphere, $h = 200$ m throughout. (d) E for R1 and R1-E with only one starting point at 210°E, period 15 days and $h = 1900$ m. The rays with positive phase speed, WMRG-E and R1-E, are shown by grey lines. The rays are followed for 30 days, with the numbers 0, 1, 2 and 3 indicating days 0, 10, 20 and 30, respectively. The domain is continued on the right-hand side to 390° to show the behaviour of some Western Hemisphere waves.

Figure 4(d) gives an example of the ray tracing for the R1 wave with period 15 days and $h = 1900$ m, starting at 210°E. The wave propagates eastwards ($c_g > 0$) and has negative B around the E Pacific westerly maximum, and hence has a local E maximum there. To the east of the E Pacific duct, where B becomes positive as the westerlies decrease, E varies in the opposite sense from U, with a maximum between the two westerly ducts and a minimum in the Atlantic duct, and accumulation near 360°E where c_g tends to zero. R1-E waves have B and c_g positive and propagate to the east with minimum E in westerly maxima, and maxima or accumulation in weak westerlies, as in Figure 4(c).

Comparison with observed wave E distributions will be given in section 4. In HY16 it is shown that the 1-D propagation theory can explain the observed WMRG and R1 wave distribution well in the Eastern Hemisphere. However the failure of free-wave theory to explain the observed maxima in WMRG and R1 wave activity in the westerly maxima regions in the Western Hemisphere is a major driver to consider the forcing from higher latitudes in these regions.

3.2. Response to subtropical forcing

Zhang (1993) and Hoskins and Yang (2000) have shown that zonally propagating forcing in the subtropics can lead to a response in equatorial waves if their damping is not too strong. The frequency of the forcing does not have to match exactly that of the free equatorial waves (i.e. resonance) in order to give a significant response – a large response to forcing is possible provided the frequency difference between the forcing and the natural frequency of the wave is not large. For example, following Zhang (1993) and Hoskins and Yang (2000), consider forcing of a zonal Fourier component, f_k, of a wave with a natural frequency ω_k by a forcing with Fourier component g_k and frequency ω_0. If the wave is Doppler-shifted by a basic flow U then, in the presence of damping α, the amplitude of the response is determined by αA, where

$$A^{-2} = 1 + \{\omega_0 - (\omega_k + kU)\}^2/\alpha^2. \quad (9)$$

Examples for a range of basic zonal flows from medium easterly to strong westerly and for eastward and westward forcing on a

time-scale of 10 days are given in Figure 5. Here the damping time-scale, α^{-1}, is taken to be 10 days. For eastward forcing (Figure 5, upper row), the response in westward-moving waves is larger for a weak westerly background wind. For strong westerlies the response is strong but mainly in the eastward-moving waves. For westward forcing (Figure 5, lower row) the WMRG comes closer to resonance and gives a larger response within the band of wavelengths of interest for stronger westerly flows. The natural westward speed of the R1 wave is much smaller and so it gives a large response over a range of wavelengths in zero flow or weak westerlies. For strong westerlies there is a significant response in the eastward-moving WMRG-E and R1-E waves. For easterly winds there is a large response only for westward forcing and for long wavelength westward-moving R1 waves which are close to resonance.

3.3. Equatorward propagation from middle latitudes and absorption and reflection

A number of studies show that equatorward propagation of extratropical waves can excite tropical waves (e.g. Webster and Holton, 1982; Kiladis, 1998; Matthews and Kiladis, 1999; Yang *et al.*, 2007c; Yang and Hoskins, 2013). The meridional propagation of Rossby wave activity is proportional to the product of the zonal and meridional wave numbers (Hoskins and Karoly, 1981). Including a wave amplitude squared factor, meridional propagation can be measured by the horizontal momentum flux $[u^* v^*]$. The brackets normally refer to a zonal average and the star to a deviation from this. With a variation of the ambient flow with longitude, a more local definition of the average defined by the bracket is more appropriate for the present purpose. In this article the brackets will refer to a region averaged between 60° west and east of the v extremum in the region of interest, and the star will refer to the deviation from this.

It will turn out to be useful in the analysis to be able to diagnose the absorption and reflection of Rossby waves. Following, for example, Hoskins and Karoly (1981) and Yang and Hoskins (1996), and considering slowly varying nearly zonal flow on the sphere, Rossby wave propagation for a particular zonal wave number k is possible if it is possible to choose meridional wave
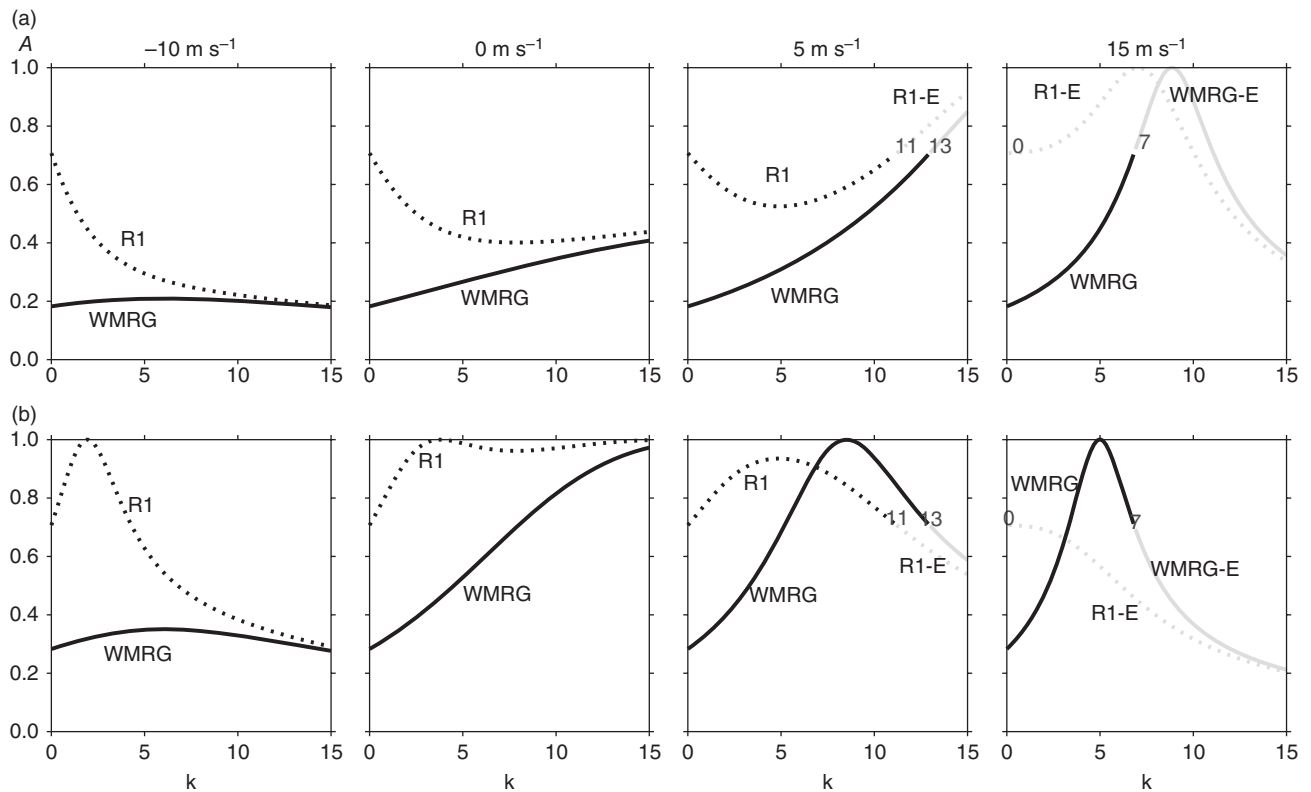
Figure 5. The response amplitude factor, A, defined in Eq. (9) as a function of zonal wave-number k for ambient zonal winds $-10, 0, 5, 15\,\text{m s}^{-1}$ (left to right columns) and for (a) eastward and (b) westward with periods of 10 days. The damping time-scale α^{-1} is also taken to be 10 days. The continuous lines refer to WMRG (black) and WMRG-E (grey) and the dotted lines to R1 (black) and R1-E (grey). The numbers refer to the wave number of transition between westward and eastward waves.

number l such that

$$k^2 + l^2 = K_m{}^2 = \frac{\beta_m}{U_m\text{-}c}.$$

Here Mercator coordinates are used with $U_m = U/\cos(\varphi)$, and β_m is the relevant latitudinal absolute vorticity gradient modified by the curvature of the basic zonal flow (see Hoskins and Karoly (1981) for details). Where $U_m - c$ goes to zero, referred to as a critical line and corresponding to $k = k_c$, the implied l becomes infinite and wave absorption is predicted. Where $K_m = k$, which will be denoted by $k = k_r$, l becomes zero and reflection is predicted. In particular if the meridional gradient of absolute vorticity is zero, then β_m is zero and all zonal wave numbers are reflected before this latitude.

4. Observed variations of equatorial waves with ENSO and the relevance of free-wave theory

4.1. Observations

Figure 6 shows vertical sections of the equatorial (7°N to 7°S) zonal wind (Figure 6(a)) and the standard deviations of the meridional wind for the WMRG, WMRG-E, R1 and R1-E wave components (Figure 6(b−e)), averaged for seven EN winters (left), seven LN winters (centre) and the difference between them, EN − LN (right). The main features in the upper tropospheric winds in both the EN and LN are the easterlies in the Indian Ocean−West Pacific (IOWP) sector, particularly near 120°E, and the westerlies in the E Pacific and Atlantic sectors. The lower tropospheric winds tend to have the opposite signs. The difference shows the large variation in all these features with ENSO, with the IOWP easterlies and E Pacific westerlies being weaker and the Atlantic westerlies stronger in EN. The magnitudes of the extrema in the upper tropospheric winds and in the difference field are given in Table 1. Also evident in Figure 6(a) is that in the LN phase the westerlies extend westwards through the date-line.

All the waves show much reduced amplitude (represented by standard deviation) below 500 hPa, with this being particularly marked for the WMRG-E. Consequently, the focus of the analysis will be on the upper tropospheric extrema in the three regions.
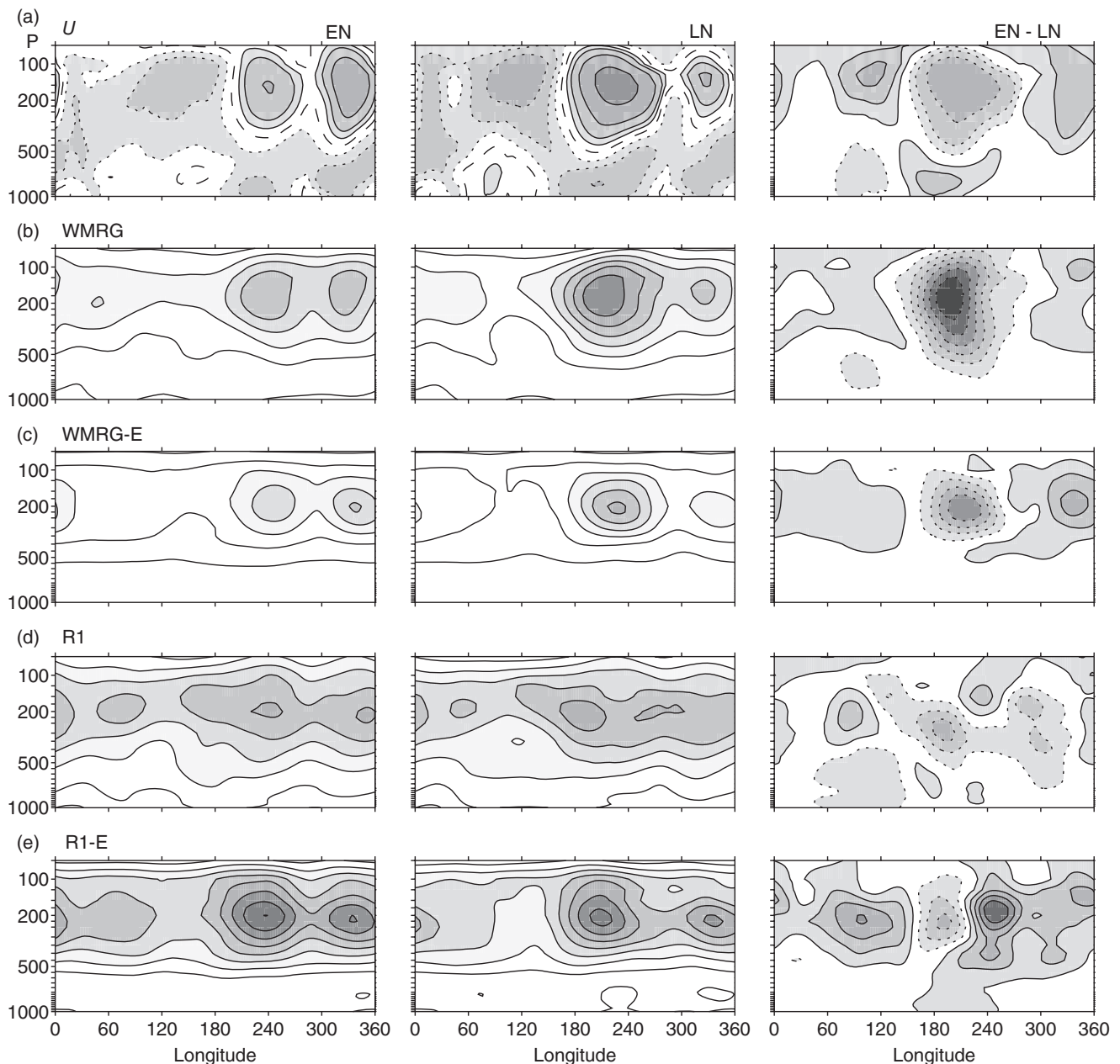
The WMRG and WMRG-E waves have slightly more intense IOWP minima and larger E Pacific maxima in LN, whereas the Atlantic maxima are larger in EN. In LN, the large values in the E Pacific extend westwards beyond the date-line. In EN the large Atlantic values for the WMRG extend to higher levels. ENSO changes in R1 and R1-E are slightly more complex. The minimum in R1 and R1-E activity in the IOWP is more marked in LN, particularly R1-E. In the E Pacific the maximum in both waves is shifted eastwards in EN, but the intensity is slightly stronger in LN for R1 and EN for R1-E. There is a large shift in the Atlantic maximum activity in R1, from the west of the westerly region in LN to the east of the region in EN. However, for R1-E here there is little shift in the Atlantic but an intensification and an increase in the upward extent of high wave amplitude in EN.

Analysis shows that the two strongest EN winters, 1982/1983 and 1997/1998, have the weakest standard deviation in all the waves in the E Pacific. This is consistent with the fact that these two EN winters have the weakest westerly ducts in the E Pacific (Yang and Hoskins, 2013).

To examine the overall importance of the gravest equatorial wave components, the percentages of the westward- and eastward-moving variance explained by each wave have been averaged for the 20°N to 20°S, 150−250 hPa region in the Western Hemisphere. It is found that the WMRG and R1 waves together explain nearly 50% of the westward-moving variance in both ENSO phases, and the WMRG-E and R1-E waves together explain at least 40% of the eastward-moving variance.

4.2. Relevance of free-wave theory

The likely importance of the direct impact of the variation of the equatorial zonal flow variation on the existence and 1-D propagation of free equatorial waves in giving the observed

ⓒ 2016 The Authors. *Quarterly Journal of the Royal Meteorological Society* published by John Wiley & Sons Ltd on behalf of the Royal Meteorological Society.

Q. J. R. Meteorol. Soc. (2016)

Figure 6. Longitude–height cross-section of equatorial zonal wind and wave standard deviations for EN (left), LN (centre) winters and the difference, EN minus LN (right). The ordinate is marked with pressure in hPa and the abscissa is longitude with tick marks every 60°. The unit throughout is m s^{-1}. (a) Zonal wind averaged 7°S to 7°N. Contours in all three fields are at 0, ±2.5, ±5, ±10, 20 except that the zero contour is suppressed in the difference field. (b) and (c) the amplitudes of the WMRG and WMRG-E waves, respectively, as measured by the standard deviation of the associated wind on the Equator. The contour intervals for the full fields are 0.4 with the lowest contour shown in each being at the value 0.4. For the difference fields the contour intervals are 0.2, with the first contours being at ±0.1. (d) and (e) give similar fields for R1 and R1-E, respectively. Here the standard deviations are for the associated v at 8°N. The contour intervals are halved, being 0.2 in the full fields and 0.1 in the difference fields with the first contours at ±0.05. In all panels, contours at positive values are continuous and those at negative values are dotted.

Table 1. The upper tropospheric extrema for equatorial zonal winds and equatorial wave variances.

Variable or wave	IOWP (90−120°E)		E Pacific (180−260°E)		Atlantic (300−360°E)	
	EN/LN	difference	EN/LN	difference	EN/LN	difference
U	−7.7/−17.4	10.4	10.3/27.1 Near 180° easterlies in EN	−19.9	19.2/10.4	9.9
WMRG	1.0/0.8	0.3	2.3/3.2 Shifts east in EN	−1.3	2.3/2.1 Extends up in EN	0.2
WMRG-E	0.9/0.6	0.3	1.9/2.5	−0.9	2.0/1.5	0.6
R1	0.8/0.7	0.2	1.2/1.3	−0.3 (188E), 0.2 (234E)	1.2/1.2 Shifts east in EN and west in LN	−0.16 (300E), 0.1 (360E)
R1-E	0.9/0.6	0.4	1.8/1.7 Shifts east in EN	−0.3 (192E), 0.5(248E)	1.6/1.4 Extends up in EN	0.3

The extrema is averaged for 150−250 hPa with unit m s^{-1}. They are shown in three regions for EL, LN and the maximum difference between them (EN − LN). The numbers in EL and LN are minimum values in IOWP and maximum values in other regions. For R1 and R1-E if the difference has two centres their longitudes are indicated. Note that the longitude ranges for these regions are slightly different from those used in later sections.

behaviour will now be considered. The focus is on the implications of possible Doppler shifting by the ambient upper tropospheric wind. The underlying assumption for this is that even though the actual flow varies in longitude, latitude and height, Doppler shifting by the ambient local westerly wind may give insight into the possible free-wave behaviour. Consider first WMRG and WMRG-E waves. As seen in Figure 3(a) the easterly flow in the IOWP region is not favourable for the existence of either wave there. However, the weaker easterlies in the EN give more possibility for the occurrence of free WMRG waves consistent with the weaker minimum in that phase that is observed. Considering WMRG waves near the date-line, a change from easterly to weak westerly allows free WMRG waves to occur over the band of wave numbers and frequencies of interest. This is consistent with the observed decrease in WMRG activity near the date-line in the EN phase. Similarly the upward extension of WMRG activity in the Atlantic is consistent with free waves in the flow that becomes westerly there in EN. For WMRG-E waves stronger westerly winds give a shift from shorter to longer wavelengths and an increase in the range of wavelengths for which free waves can occur. The increased WMRG-E activity with the strong westerlies in the E Pacific with LN and the Atlantic with EN are therefore consistent with free-wave changes. However, the similar changes in WMRG activity are not simply explained in this way.

On the basis of Figure 3(a), the existence of the WMRG-E in EN may be doubted since the equatorial U (Figures 2(a) and 6(a)) appears to be too weak. However, such waves are indeed theoretically possible during EN, because of the variability in the zonal wind field. The zonal winds shown in Figures 2(a) and 6(a) are the averages of seven EN and seven LN winters (November to April). During some periods, especially in December to February, the zonal wind is much stronger than the mean of the seven seasons, and even for EN the zonal wind maximum can exceed 15 m s^{-1}. Ten-day average equatorial U across the E Pacific has been calculated, assuming that this time-scale can be considered to be the ambient zonal flow on which the waves propagate. Averaged over the years, the standard deviation of U in the upper troposphere is found to be about 90% of the mean in EN winters and 60% in LN winters.

Free-wave changes explain only a few features of the observed variations in R1 and R1-E activity. The slightly weaker amplitude in R1 activity in the IOWP for the LN with its stronger easterlies is consistent. However the variation in the minimum in R1-E is even more marked, though free R1-E waves should not occur for even the weaker easterlies in the EN phase. The Atlantic intensification of the R1-E maximum in the EN with its stronger westerlies there is consistent with the possible occurrence of free waves, as is its upward extension in the region of westerlies. However, other variations in R1 and R1-E do not seem to be simply related to the possibility of free waves.

Considering the 1-D propagation theory, in the Eastern Hemisphere the theory suggests slightly weaker energy as WMRG waves propagate westwards from near 120°E towards weaker easterlies (Figure 4(b)). This seems to explain the observed amplitude decreasing from 120°E to 90°E but has little relevance to the general picture there or the EN−LN difference, nevertheless the energy is small in this region (Figure 6(b)). On the other hand, the propagation theory (Figure 4(c)) predicts that R1 waves will have significantly increased energy as they propagate westwards from the region of strong easterlies towards the region of minimum easterlies. This is in agreement with the local maximum near 60°E seen in both EN and LN in Figure 6(d).

However, it is the Western Hemisphere maxima that dominate the distributions of all the waves. 1-D propagation theory (Figure 4(d)) seems to be able to predict some features of the observed R1 waves. Figure 4(d) shows that R1 waves with lower frequency and larger h can have a local maximum in the westerly duct (supposing the westerly is not too strong so the wave can exist). This is in agreement with the observed local R1 wave maximum in the E Pacific duct, especially in EN (Figure 6(d)).

The propagation theory also suggests a local maximum between the two westerly ducts, which is again consistent with the observed R1 maximum there in LN. In addition, the theory suggests the wave accumulating around 360°E, which is also consistent with the observed R1 peak there in EN, although the peak is weak. However, for the other three waves in the Western Hemisphere, the 1-D propagation theory is not able to predict their behaviour. Figure 4(b) and (c) give that the wave energy of WMRG, WMRG-E and R1-E waves should amplify strongly and their wavelengths shorten as they propagate eastwards from the westerly maxima in the E Pacific to the minimum westerlies near 280°E, and as they propagate eastwards from the Atlantic westerly maximum they should accumulate near the 360°E zero in U. In contrast, the observed maximum wave amplitudes for all three waves are in the regions of the westerly wind maxima. In partial agreement with the 1-D propagation theory, in HY16 it is shown that higher wave numbers in the band 11−30 do indeed have maxima that are shifted east of the westerly wind maxima, but the amplitudes are small compared with the band 2−10. In addition it is the ENSO phase with strongest westerlies that has the largest amplitude for the WMRG and WMRG-E waves.

5. Forcing from higher latitudes

Given the failure of free-wave propagation to explain the observed WMRG, WMRG-E and R1-E maxima that are found in the Western Hemisphere, we now turn to the second major aim of this article, which is to examine the importance of higher-latitude forcing in this region for explaining the Western Hemisphere maxima and their variation with the phase of ENSO. As discussed in section 3.2, and as shown in Figure 5, low-frequency forcing gives the largest response for waves whose natural frequencies differ little from the forcing. For westward forcing, the WMRG waves in the band of interest in the E Pacific are closer to resonance for the stronger westerlies in the LN phase and in the Atlantic for the EN phase. The observed larger activity in WMRG-E for the stronger westerly phase of ENSO in the E Pacific and Atlantic could be the response to eastward-moving forcing as indicated by the top right panel in Figure 5. As there would be a large R1 response to westward forcing for weak westerlies and a large R1-E response for strong westerlies to both westward and eastward forcing, such forcing could be important for the variation of these waves.

5.1. Eastward-moving waves

In regions of strong westerlies WMRG-E waves could be driven by lateral eastward forcing associated with eastward-moving waves in the subtropics. In strong westerly regions it could also be driven by extratropical wave trains propagating meridionally into the equatorial region. To diagnose the latter, the momentum flux associated with eastward-moving variance in the upper troposphere is regressed onto the extrema of WMRG-E equatorial v at 200 hPa in the E Pacific and Atlantic sectors, and the results are shown in Figure 7(a) and (b). In the NH subtropics, as seen in Figure 2, the eastward-moving variance in v is larger in EN. However in the E Pacific, consistent with the stronger westerly duct in LN, it is this season in which the propagation from the NH into and across the Equator is much larger (larger positive $[u^\star v^\star]$). In the Atlantic it is the EN season that has the strongest westerly duct and the strongest equatorward propagation from the NH, though here only to about 5°N.

To examine the synoptic structures associated with large WMRG-E activity, full eastward-moving u, v and Z are regressed onto extrema in WMRG-E equatorial v with lags −2, 0 and +2 days. The results are shown in Figure 7(c)−(e), for the latitude range 30°N−30°S, which is broader than that used to determine the equatorial waves themselves.

Looking first at zero lag, although the fields of u, v and Z do not use data that has been projected onto equatorial wave
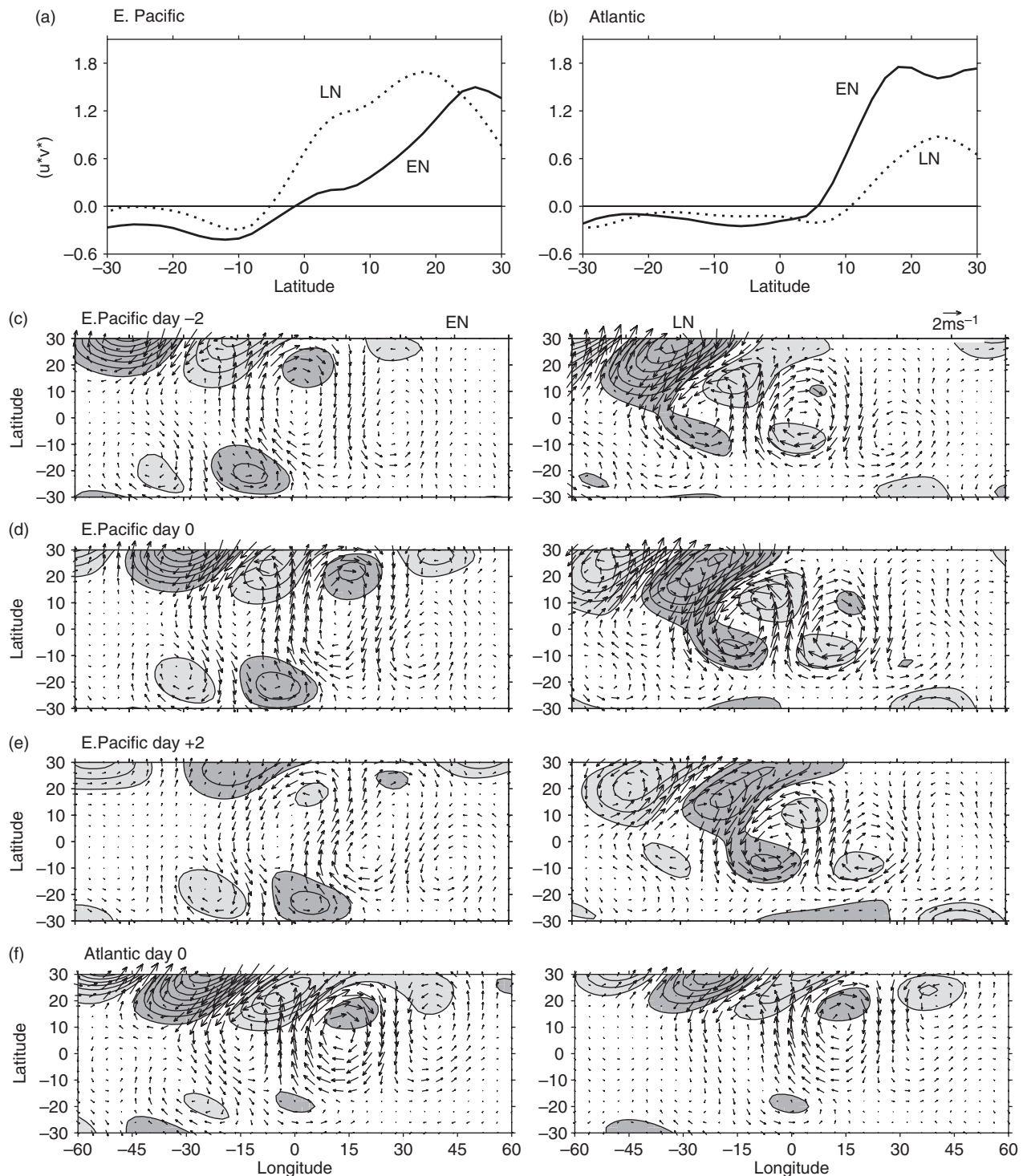
Figure 7. (a) and (b) Horizontal eddy momentum flux [u*v*] regressed onto the extrema of 200 hPa WMRG-E equatorial v, averaged on 100–300 hPa and −45° to 15° longitude range, for (a) the E Pacific (220–260°E), and (b) Atlantic (310–350°E), for (solid) EN and (dotted) LN winter. Units are m² s⁻². (c–e) 200 hPa eastward-moving horizontal winds (vectors) and geopotential height Z (shading), regressed onto the extrema of 200 hPa WMRG-E v over the E Pacific at lag day −2, 0 and +2. (f) As (c–e) but for zero-lag fields for the Atlantic. The dark (light) shading is for positive (negative) Z, with a contour interval 2 m and the zero contours are not drawn. The extreme v is taken to be southerly and located at 0° relative longitude, with a positive value of 1.5 times its peak standard deviation.

structures, the regressed field in the tropical region is dominated by a WMRG-like wave structure, with rotational flow centred on the Equator. Subtropical wave trains are seen, mainly in the NH and to the west. Consistent with Figure 7(a), the LN picture clearly exhibits greater propagation into the equatorial region. This is consistent with the proposal of Webster and Holton (1982) and the results of Yang and Hoskins (1996) that showed in an idealized model that midlatitude non-stationary eastward-moving Rossby waves can propagate into the equatorial region in the presence of strong westerly flow. The lagged pictures emphasise that the subtropical wave trains propagate from the west and that the phase propagation and development in the subtropics and the Tropics are towards the east. Because of its structure and eastward phase

speed, the tropical pattern will be referred to as WMRG-E. The EN WMRG-E is seen mainly as a response to subtropical forcing by the wave train, whereas the larger amplitude of WMRG-E in LN has the additional direct forcing by the propagation into the equatorial region. The zero-lag pictures for the Atlantic (Figure 7(f)) shows similar results. Meridional propagation occurs for the stronger westerly duct which now occurs in EN. However, consistent with Figure 7(b), the propagation does not appear to reach the Equator. The subtropical forcing gives a WMRG-E response in LN but this is weaker than in EN when the more direct forcing occurs.

Similar diagnostics for R1-E are given in Figure 8. In the E Pacific, the northern subtropical variance is larger in
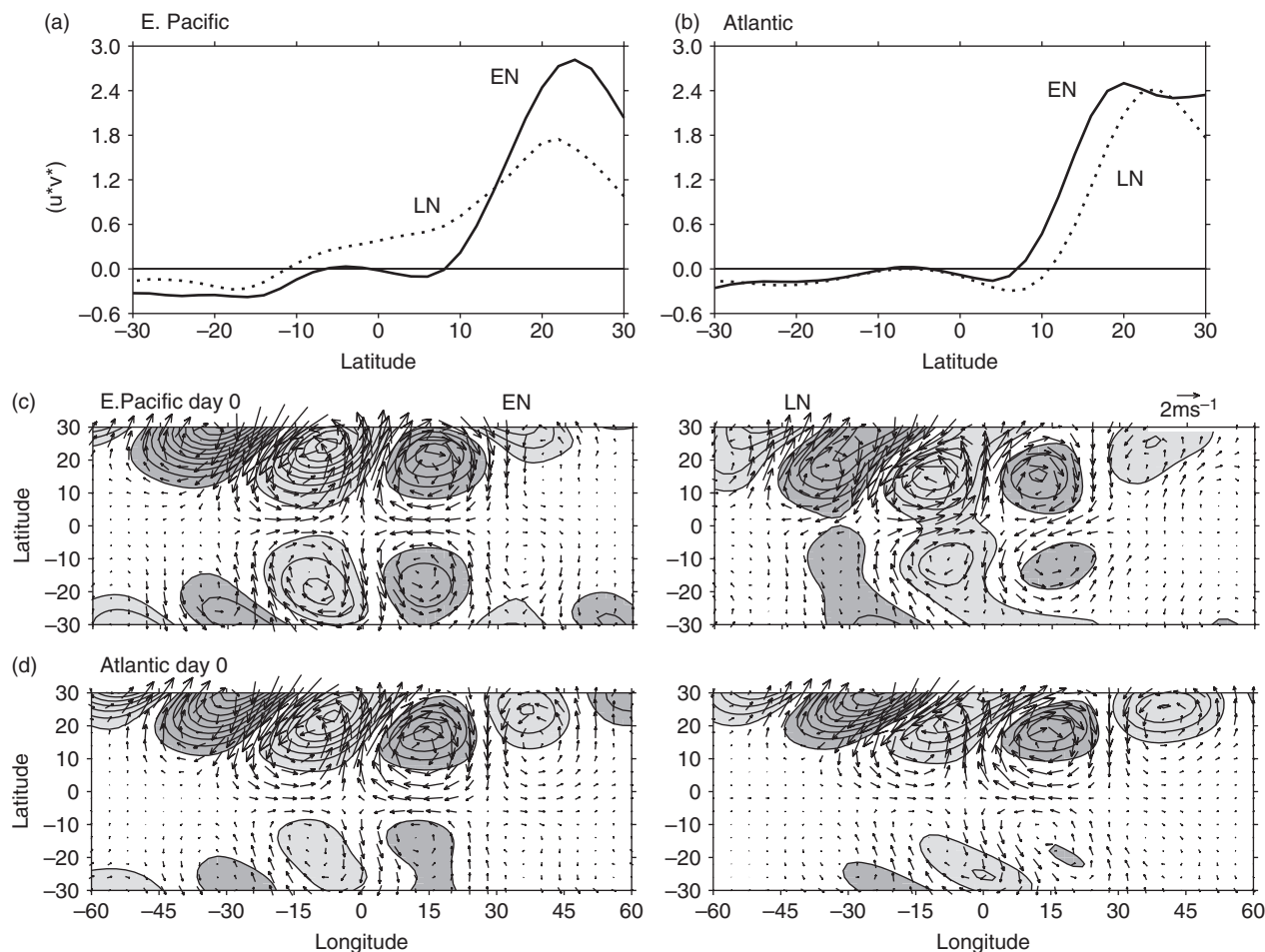
Figure 8. As Figure 7 but for fields regressed onto 200 hPa R1-E off equatorial *v* at 8°N. (a) and (b) momentum fluxes for the E Pacific and Atlantic, respectively. (c) and (d) Zero-lag regressed wind and height fields for the E Pacific and Atlantic, respectively.

EN (Figure 2(b)), but the equatorward propagation is more significant in LN (Figure 8(a)). In the Atlantic (Figure 8(b)), the equatorward propagation from the NH reaches closer to the Equator in the EN phase. Regressed horizontal fields (Figure 8(c) and(d)) are dominated by R1-E-like structures. The regressed fields at zero lag for the E Pacific (Figure 8(c)) show wave trains in the subtropics of both hemispheres, with the northern train being stronger. In LN winters the equatorward propagation of the wave train and its connection with the R1-E structure is clearly seen. This is consistent with Yang and Hoskins (2013) where the horizontal structure regressed on the Kelvin wave in LN also indicates the presence of an eastward-moving R1 wave structure. In agreement with Figure 8(a), there is little sign of meridional propagation between 15°N and the Equator in EN. There appears to be some propagation into and then out of the Equator in the SH, which is therefore not seen in the momentum flux diagnostic. However, the suggestion from these diagnostics is that the R1-E wave in the E Pacific in EN is driven mainly by lateral forcing. Propagation from the NH into the deep Tropics is apparent in LN and there are indications of a WMRG-E wave there. The Atlantic differences in the two ENSO phases are not large, though stronger equatorial wind perturbations occur in EN, consistent with the stronger equatorward propagation being important.

It is of interest to remove any dependence on the projection onto the resting atmosphere equatorial waves and look at the regressed wave structures in a similar manner. The wind fields used will be the raw data with only their time mean removed. Figure 9 shows pictures for this full wind field, regressed onto eastward-moving extrema in *v* in the E Pacific region at the Equator for day −2 and 0 and at 16° north and south at day 0. A large longitudinal and latitudinal domain is used to show more clearly the connections between the tropical and extratropical regions. Importantly, the lower-latitude circulation in the grey

box in Figure 9(a) and (b) is seen to be almost identical to that in Figure 7(c) and (d). This indicates that the WMRG-E is indeed capturing the important variance in the equatorial region. Also it is apparent from Figure 9(a) and (b) that eastward-propagating midlatitude wave activity propagates into the Tropics and leads to eastward-moving MRG structures there. Comparing Figure 9(c) and (d) with Figure 8(c), using the *v* extrema at 16°N and 16°S separates the contributions to R1-E from the wave trains in the two hemispheres. In addition, both show indications of a WMRG-E structure in the stronger westerly duct in LN. It should be noted that the standard deviation of *v* at 16°N is about 50% greater than that at 16°S (Figure 2(b)) which explains the smaller contribution of the southern wave train in Figure 8(c). Figure 9(b) and (c) suggest that the northern extratropical wave train that forces WMRG-E typically has a longer wavelength (60°) than the one that typically forces the R1-E wave (48°). However Figure 9(c) and (d) show that the WMRG-E and R1-E waves can occur in combination.

The very close similarity of these results, obtained based on totally unfiltered fields, with those obtained using the equatorial wave structure projection technique strongly supports the validity and usefulness of that technique. In particular there is confirmation that the eastward-moving results found using the equatorial wave projection technique are in no way due to the aliasing of midlatitude variability.

5.2. Westward-moving waves

The westward-moving *v* amplitude varying with ENSO phase was shown in Figure 2(c). The subtropical amplitudes are about half those for eastward moving *v* (Figure 2(b)). However, the tropical values and their variation with ENSO phase are similar for eastward- and westward-moving variance.
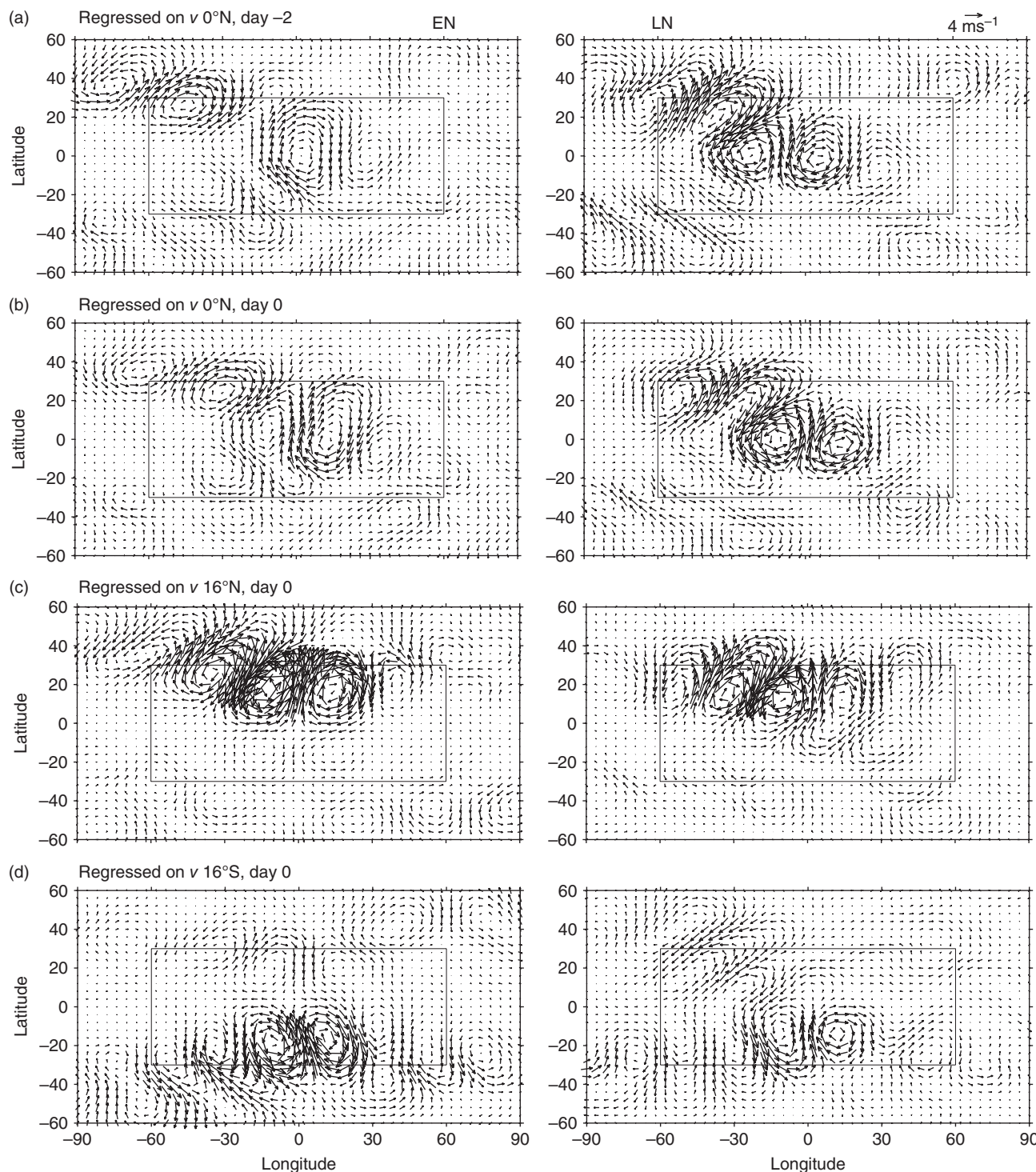
Figure 9. Full winds (with only the time mean removed) regressed onto 200 hPa total eastward-moving *v* extrema at (a) 0° for day −2; (b) 0° for day 0; (c) 16°N for day 0, (d) 16°S for day 0. The grey box indicates the longitude and latitude domain in Figure 7. Conventions as in Figure 7 but with the wind vector scale being doubled.

Figure 10 shows wave forcing diagnostics for the WMRG wave, obtained by regressing full westward-moving fields onto the extrema of WMRG equatorial *v*. The values of momentum flux are about four times smaller than those for the eastward-moving waves. In the E Pacific the SH values are now the largest. The indications of propagation towards the Equator are again larger in LN with its stronger westerlies. Figure 10(c) gives the flow regressed onto WMRG *v* extrema with zero lag. Lagged fields (not shown) indicate that the westward-moving subtropical wave trains have an eastward group velocity, as was the case for the eastward-moving wave trains. Consistent with Figure 10(a), the SH wave train is clear in both ENSO phases but there is almost no NH wave train in the EN phase. It is interesting to note that the SH wave train arches into and out of the Tropics with little asymmetry in amplitude. In such a situation more

akin to reflection, the propagation into the equatorial region is considerably underestimated by the momentum flux diagnostic. The WMRG-like wave is apparent in both phases but is stronger in LN. The zonal wavelength, about zonal wave-number 5, is longer than for the eastward-moving waves, consistent with the suggestion from Figure 3(a). The connection of the WMRG with a SH subtropical wave train seen here is consistent with Magaña and Yanai (1995).

In the Atlantic, the momentum flux diagnostic suggests propagation from both hemispheres, but mainly from the SH in EN and from the NH in LN (Figure 10(b)). The regressed fields (Figure 10(d)) confirm this and show larger tropical response in the stronger westerly in EN.

For westward-moving fields regressed onto the R1 wave (Figure 11), in the E Pacific wave activity propagation is indicated
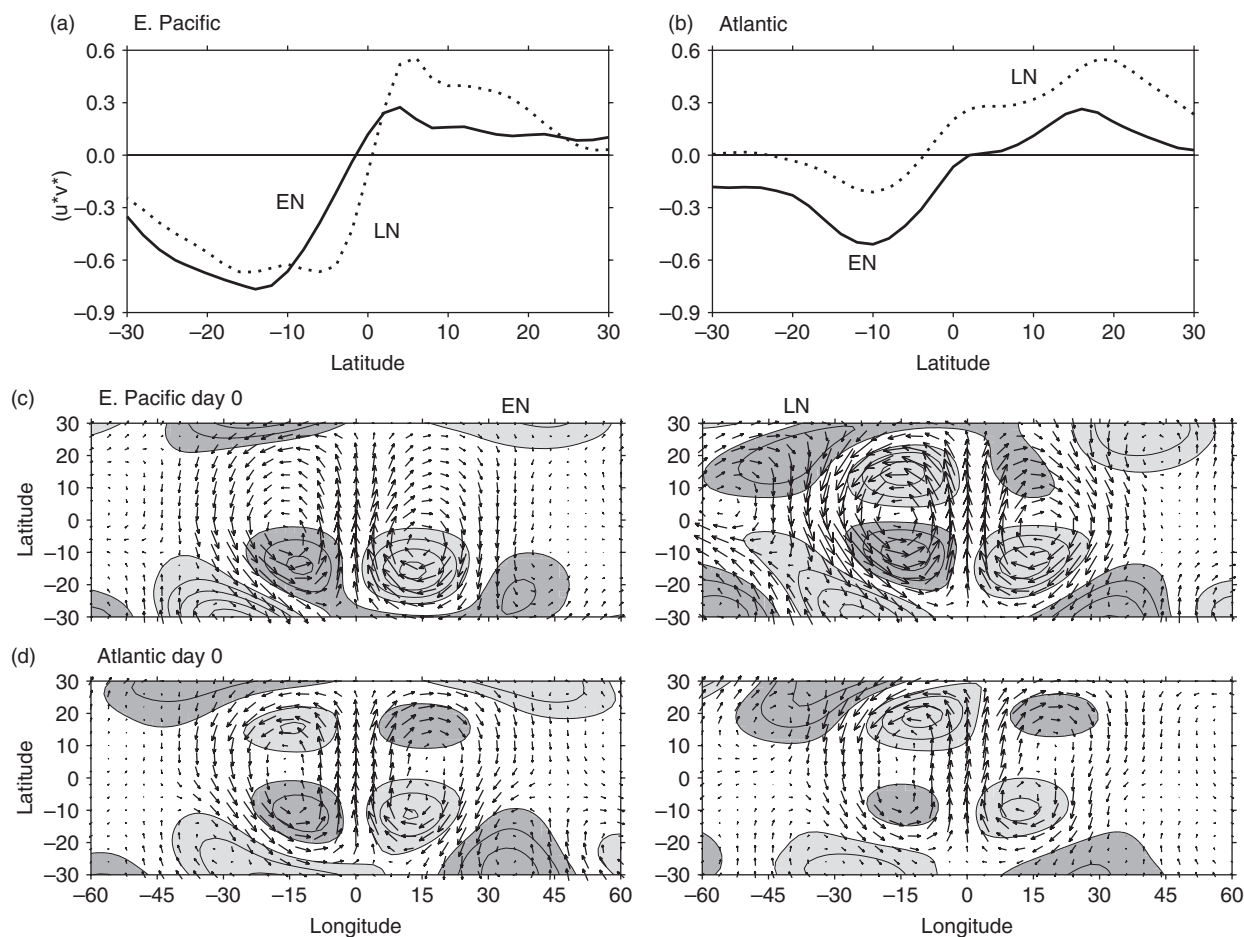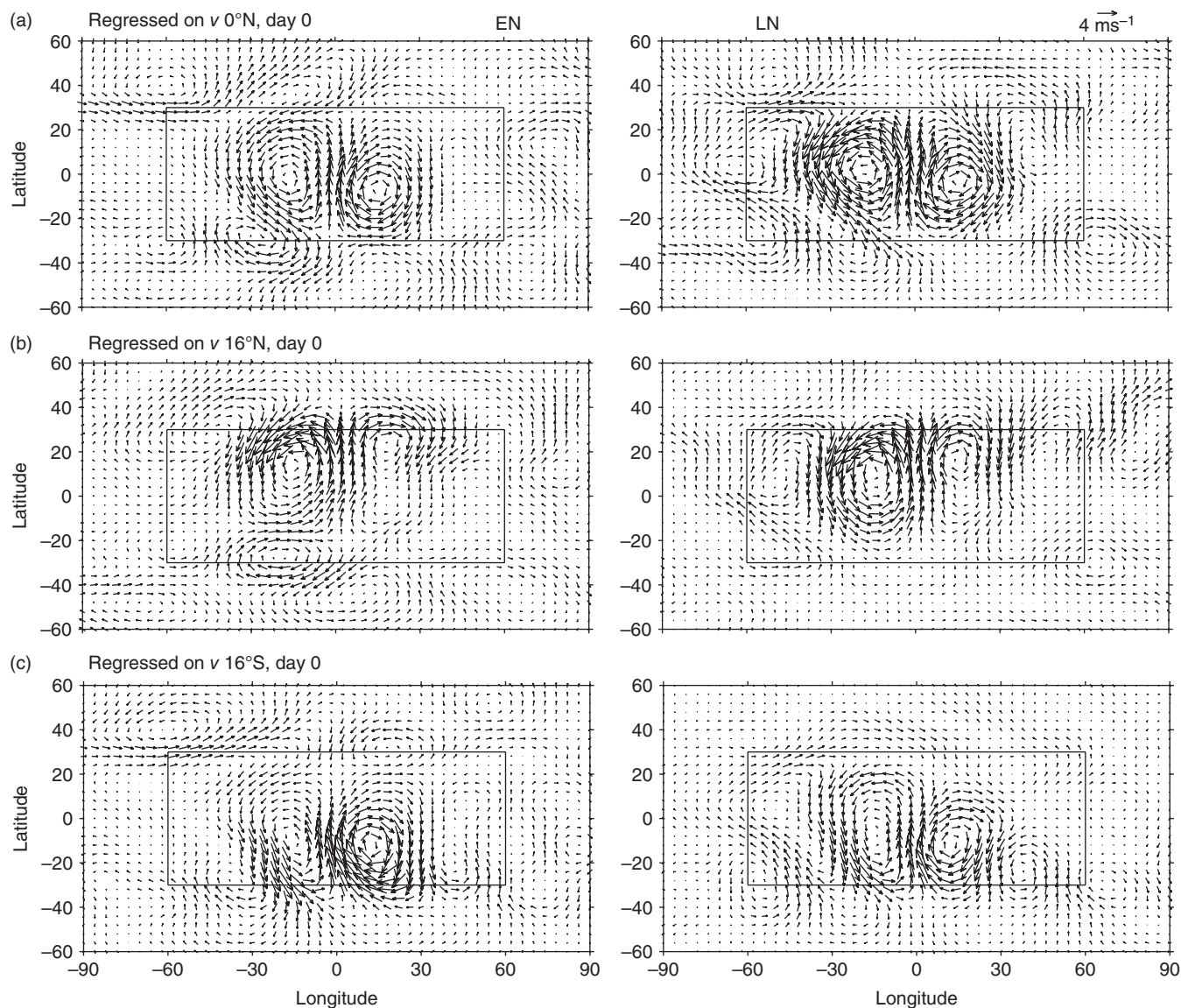
Figure 10. As Figure 7 but for fields regressed onto 200 hPa WMRG equatorial *v* at zero lag. (a) and (b) Momentum fluxes for the E Pacific and Atlantic, respectively. (c) and (d) Zero-lag regressed wind and height fields for the E Pacific and Atlantic, respectively.
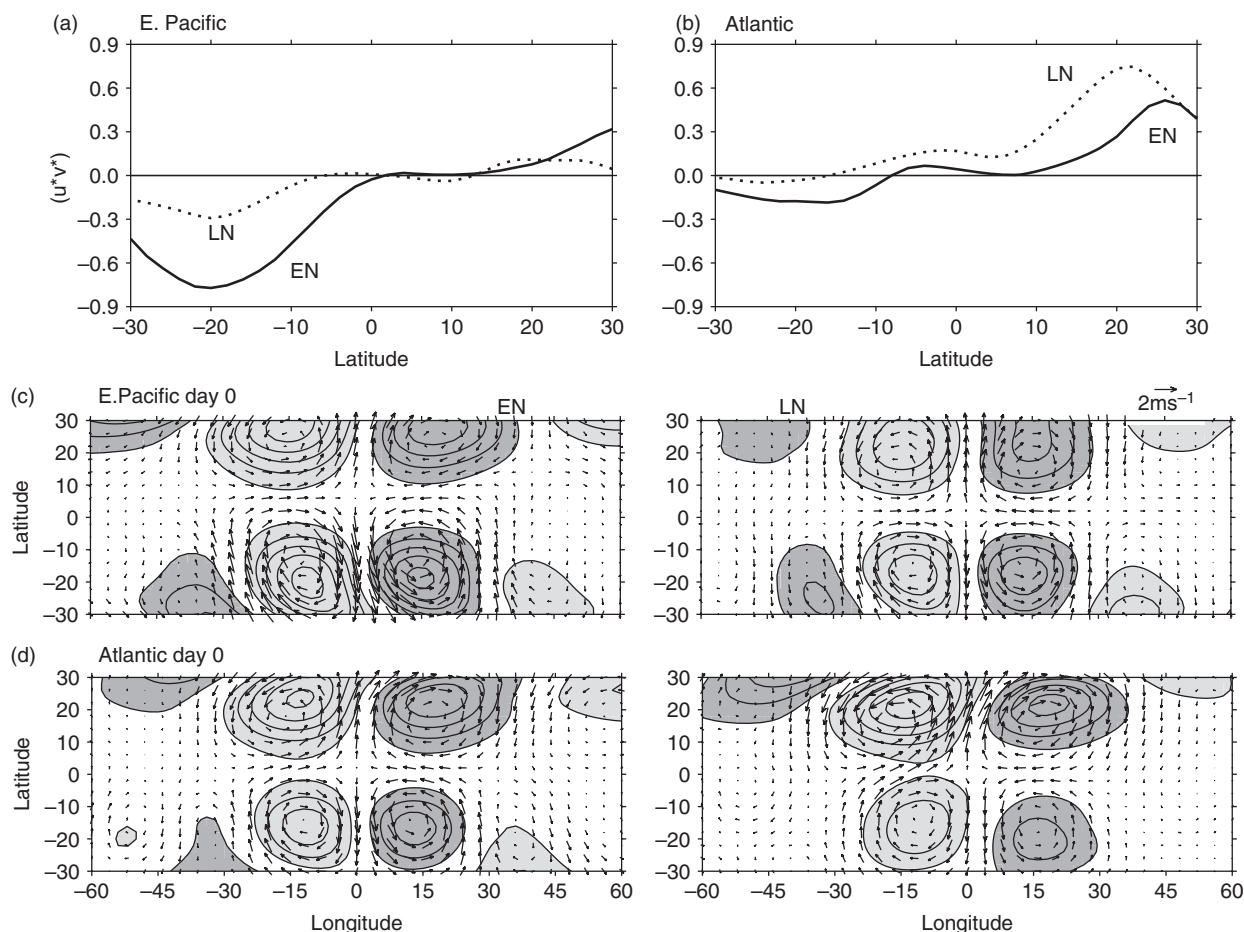
Figure 11. As Figure 7 but for fields regressed onto 200 hPa R1 off-equatorial *v*. (a) and (b) Momentum fluxes for the E Pacific and Atlantic, respectively. (c) and (d) Zero-lag regressed wind and height fields for the E Pacific and Atlantic, respectively.

Figure 12. As Figure 9 but for full winds regressed onto 200 hPa total westward-moving v extrema at (a) 0°N, (b) 16°N and (c) 16°S, for day 0.

as being quite weak but at its strongest in the SH and in EN (Figure 11(a)). The regressed fields again show near symmetry of the SH subtropical waves up- and down-stream, but the tilts of the waves are smaller than for the WMRG. The SH component of R1 is stronger in the EN phase, but there is near hemispheric symmetry in LN (Figure 11(c)). In the Atlantic, NH meridional propagation is now emphasised in the momentum flux diagnostic in LN (Figure 11(b)). In this region it is this ENSO phase that emphasises the R1 structure in one hemisphere, this time the NH, with the EN pattern being more hemispherically symmetric (Figure 11(d)). In the LN phase there is some cross-equatorial flow, which could be interpreted as evidence of a WMRG response. The zonal scale of the waves in the NH is about wave-number 5, again longer than for the eastward-moving wave. This is consistent with Figure 3(b). However the SH wave is shorter, about wave-number 7. This is also consistent with Figure 3(b) due to the generally weaker subtropical westerlies in the SH.

Figure 12 gives the fields for full winds in a large domain regressed on westward-moving v extrema in the E Pacific region at the Equator and at 16° north and south for the two phases of ENSO. As was the case with eastward-moving activity, in Figure 12(a) the circulation in lower latitudes is almost identical to that for the WMRG related v extrema (Figure 10(c)). Again this strongly supports the validity and usefulness of the projection technique. The two 16° latitude pictures (Figure 12(b) and (c)) again separate the two hemispheric contributions to the R1 (Figure 11(c)). In each the subtropical wave train extends across

the Equator to 15°−20° latitude in the other hemisphere in what can be described as an R1 plus WMRG wave. As was the case in Figure 11(c), the wavelength in the NH (Figure 12(b)), with its stronger subtropical westerlies, is greater than that in the SH (Figure 12(c)). From these results, a better perspective than a simple R1 wave may be a wave in one or other hemisphere that extends up to and across the Equator in an R1 plus WMRG-like structure.

6. Summary and concluding comments

The amplitudes of the gravest equatorial waves in the troposphere having a v component, i.e. $n = 0$ and 1, have been documented for the two phases of ENSO in the NH winter, along with the difference between them. To our knowledge it is the first such study. In particular the eastward-moving variance in the upper troposphere has been found to be dominated in the Western Hemisphere by WMRG and R1 structures that appear to be Doppler-shifted by the flow to move eastwards. In the E Pacific and Atlantic it is found that the strong westerly seasons, LN in the E Pacific and EN in the Atlantic, have the larger WMRG and WMRG-E amplitudes. The changes with ENSO phase of R1 and R1-E in these regions is less simple. In the E Pacific, R1 is also a maximum in LN, whereas R1-E exhibits more of an eastward shift between LN and EN. Over the IOWP, all upper tropospheric waves tend to be stronger in EN winters with their reduced equatorial easterly winds.

It has been shown using the full winds with only the time mean removed that the upper tropospheric structures associated with both eastward- and westward-moving meridional wind extrema on the Equator and in the subtropics are very similar to those associated with the projections on to the $n = 0$ and 1 waves for a resting atmosphere (Figure 9 compared with Figures 7, 8, and 12 compared with Figures 10 and 11). It is apparent that they could be largely described in terms of resting atmosphere equatorial wave and Rossby wave structures. This strongly supports the application of the projection technique for some of the analysis, and the use of the terminology WMRG and R1 for the $n = 0$ and $n = 1$ waves, respectively. Figures 9 and 12 also confirm that the results obtained using equatorial wave projections are not due to the aliasing of higher-latitude variability.

A similar analysis has also been performed for NH summer. It is found that the ENSO impact on the $n = 0$, 1 waves is significant only in the E Pacific, with WMRG suppressed and R1-E enhanced in EN summers.

The fact that EN events significantly suppress WMRG waves over the central-eastern Pacific in both winter and summer may have an implication for the stratosphere QBO. Maruyama and Tsuneoka (1988) found that EN events had a connection to longer-lasting QBO westerly/shorter-lasting QBO easterly. This is consistent with the finding here considering that the tropospheric WMRG waves, which propagate upwards and contribute to the easterly momentum acceleration, are suppressed in EN years. In addition, given that Kelvin waves contribute to the westerly momentum acceleration, the QBO difference may also be related to the fact that upper-tropospheric Kelvin waves are substantially enhanced by EN events, as shown in Yang and Hoskins (2013). A modelling study of Maury *et al.* (2013) indeed showed that ENSO has a substantial influence on stratospheric Kelvin waves.

The likely importance of the direct impact of the variation of the equatorial zonal flow on the existence and propagation of free equatorial waves in giving the observed behaviour has been examined in the context of possible Doppler shifting by the ambient upper-tropospheric zonal wind. For WMRG waves, the observed weaker minimum in EN over IOWP is consistent with the weaker easterlies in that phase. The stronger amplitude of the WMRG waves near the date-line in LN is also consistent with the flow there changing from easterly to weak westerly (allowing free WMRG waves to occur in the band of interest). Similarly the upward extension of WMRG activity in the Atlantic is consistent with free waves in the flow that becomes westerly there in EN. Increased WMRG-E activity with the strong westerlies in the E Pacific with LN and in the Atlantic with EN are consistent with stronger westerly winds giving an increase in the range of wavelengths for free waves. However, for R1 and R1-E, the free-wave changes explain only a few features of their observed variations. The slightly weaker amplitude in R1 activity in the IOWP for the LN with its stronger easterlies is consistent. The Atlantic intensification of the R1-E maximum in the EN with its stronger westerlies there is also consistent with the possible occurrence of free waves, as is its upward extension in the region of westerlies.

The 1-D propagation theory can explain some features of R1 waves. The local maximum of R1 waves near $60°$E in both EN and LN can be associated with significantly increased energy as they propagate westwards from the region of strong easterlies towards the region of minimum easterlies. The theory can also explain the local maximum of R1 waves in the weaker westerly duct in EN but on the flanks of the stronger duct in LN over the E Pacific. However, the theory fails to explain the zonal distribution of other waves and their variation with the phase of ENSO, especially in the Western Hemisphere.

The second aim of this article was to examine the forcing of equatorial waves in the Western Hemisphere from higher latitudes using the ENSO variation of the westerly winds in this hemisphere. Considering first the eastward-moving waves, the observed behaviour for WMRG-E in both the E Pacific and the Atlantic is consistent with the expectation of the stronger

Table 2. Correlation of $n = 0$ wave mode amplitude with equatorial zonal winds at 200 hPa.

Wave	CP	EP	CA-WAT	AT
WMRG-E	**0.89**	**0.70**	0.31	**0.86**
WMRG	**0.89**	**0.72**	**0.42**	**0.36**

The correlation is for four regions: central Pacific (180–220°E, CP), E Pacific (220–260°E, EP), Central America–west Atlantic (270–310°E, CA-WAT) and Atlantic (310–350°E, AT). Bold numbers indicate correlation exceeding 95% significant level, i.e. larger than 0.345.

westerly phase of ENSO giving both a stronger westerly duct for propagation from higher latitudes into the equatorial region and a larger response there. The same is true for R1-E but in this case lateral forcing by eastward-moving subtropical wave activity appears to be dominant, and this is largest for both the E Pacific and the Atlantic in the EN phase.

For the westward-moving WMRG in the E Pacific, there is empirical evidence of enhanced propagation into the equatorial region from the SH and this, along with the response, is largest in the strong westerly phase in LN. For R1 there is evidence of lateral forcing with some equatorial propagation from the subtropics in the E Pacific.

To illustrate more generally the relationship of WMRG-E and WMRG wave amplitudes with equatorial westerlies, the correlations of these amplitudes with the equatorial zonal wind in the same region for a number of sectors and averaged for all 31 winter seasons is given in Table 2. The correlation is significant for both waves in each region, except for WMRG-E in the Central America–west Atlantic. However, it is particularly large in the central and east Pacific and in the Atlantic.

The propagation of eastward-moving variance into and through the equatorial region in the westerly duct has been the subject of many studies. However, the westward-moving wave train that arches eastwards from the SH into and out of the equatorial region, where it triggers the WMRG wave, appears to be new. To diagnose this behaviour, Figure 13 gives for winter EN and LN at 200–220°E and averaged between 100 and 300 hPa the Rossby wave propagation diagnostics detailed in section 3.3. Shown in (a) and (b) are U_m and β_m, and in (c)−(f) the critical line absorption and reflection curves as a function of latitude for waves with a period of (c,d) $+10$ days (eastward-moving) and (e,f) -10 days (westward-moving). For the eastward-moving waves, the LN E Pacific wave duct is apparent. In LN (Figure 13(d)) wave numbers between 3 and 9 are able to propagate from the NH to about 8°S before they are absorbed, whereas in EN (Figure 13(c)) they are absorbed by 10°N. Of more novel interest is the behaviour for westward-moving waves in the SH (Figure 13(e) and(f)). Consistent with what has been seen in Figure 10(c), zonal wave-numbers 6 or less are reflected near 12°S, this feature being slightly more prominent in LN. This reflection is associated with a value of β_m that is close to zero in this region (Figure 13(a) and(b)). This near-zero meridional gradient in absolute vorticity is associated with the southern edge of the equatorial westerlies in LN and with the northern edge of the SH westerlies in EN. Therefore the observed behaviour of the arching westward-moving wave train in this sector is entirely consistent with the theoretical expectation of reflection there.

The most significant mechanism for the R1-E and R1 waves appears to be lateral forcing from the subtropics aided by their meridional scale. To test the more general importance of this relationship, the correlations between R1-E and R1 wave amplitudes and the standard deviation of v at 20°N and 20°S in the same sector have been determined for a number of sectors and are shown in Table 3. For both waves the lateral forcing in both hemispheres is generally important. The major exception is the SH in the central Pacific for R1-E, and for R1 there is some variation with sector over which hemisphere is more important, with NH forcing in E Pacific and Atlantic being not important.
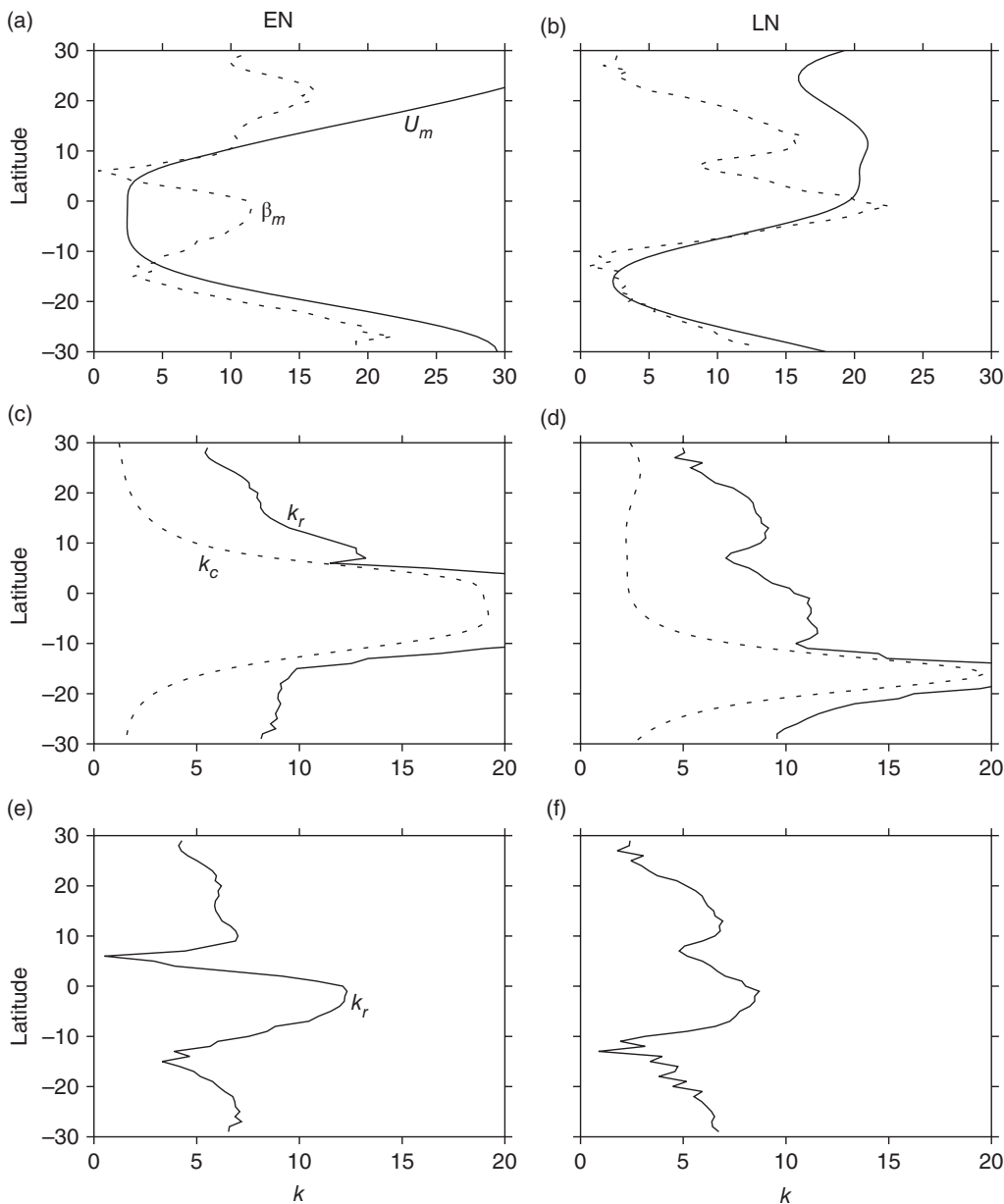
Figure 13. Rossby wave propagation diagnostics for (a,c,e) EN and (b,d,f) LN winters in the sector $200-220°E$ and averaged between 100 and 300 hPa, as presented in section 3.3. (a) and (b) U_m (continuous, unit m s^{-1}) and β_m (dashed, unit 5×10^{-12} m^{-1} s^{-1}). (c–f) The critical line absorption (dashed) wave number, k_c, and reflection (continuous) wave number, k_r, as a function of latitude for waves with a period of (c) and (d) 10 days (eastward moving), and (e) and (f) -10 days (westward moving). The abscissa is zonal wave number. Permitted waves have wave numbers less than k_r and greater than k_c. At this longitude there is no critical line for the negative period cases.

Table 3. Correlation of $n = 1$ wave amplitude with eastward- or westward-moving v amplitude.

Wave/location	v latitude	IOWP	CP	EP	CA-WAT	AT
R1-E	20°N	**0.88**	**0.72**	**0.74**	**0.65**	**0.67**
	20°S	**0.65**	0.08	**0.63**	**0.60**	0.35
R1	20°N	**0.61**	0.42	0.29	**0.68**	0.24
	20°S	**0.52**	**0.69**	**0.63**	0.36	0.45

The $n = 1$ wave amplitude is correlated with eastward- or westward-moving v amplitude at 20°N and 20°S in the upper troposphere (150−250 hPa) for various regions: IOWP (60−120°E), CP, EP, CA-WAT and AT. Conventions as in Table 2.

Lateral forcing for equatorial waves has been proposed by a number of studies for WMRG and R1 waves (e.g. Mak, 1969; Wilson and Mak, 1984; Zhang, 1993; Magaña and Yanai, 1995) and for Kelvin waves (e.g. Zhang, 1993; Hoskins and Yang, 2000; Yang et al., 2007c). However, lateral forcing for the eastward WMRG-E and R1-E has not been investigated before. This study reveals that for the gravest equatorial waves, the most significant lateral forcing occurs for the R1-E in the Western Hemisphere upper

troposphere associated with the fact that the subtropical waves are dominated by eastward-moving disturbances and also the $n = 1$ mode has a broader meridional scale than the $n = 0$ mode.

In summary, the contrasting behaviour of WMRG and R1 waves in EN and LN seasons has been documented with a focus on the NH winter. The observed variation of equatorial waves with ENSO phase has enabled an evaluation of the relative importance of various mechanisms for the amplitude of eastward- and westward-moving WMRG and R1 waves. For WMRG the importance of equatorial westerlies and the possible wave existence and response and forcing by wave propagation into equatorial westerly ducts has been highlighted. Propagation of eastward-moving wave activity in the westerly duct has been widely discussed before. However, interestingly, westward-moving wave activity arching into the deep Tropics from the SH is also more apparent with stronger equatorial westerlies. For the R1 waves, lateral forcing from the subtropics is the dominant mechanism. However, wave activity conservation and the 1-D propagation theory developed in HY16 are also important for westward-moving R1 in giving maximum amplitude in weak westerlies or on the flanks of strong westerlies.

The variation of convectively coupled waves with ENSO phase and their possible convective forcing have not been investigated in this study. It is also worthy of note that the variation of WMRG and WMRG-E waves with ENSO phase is consistent with changes in the response to stochastic forcing, possibly of convective origin (F.-F. Jin, personal communication, 2015). The role of convection in equatorial waves will be the subject of a subsequent article.

Acknowledgements

References

Bretherton FP, Garrett CJR. 1968. Wavetrains in inhomogeneous moving media. *Proc. R. Soc. London A* **362**: 529–554.

Chang H-R, Webster PJ. 1995. Energy accumulation and emanation at low latitudes. Part III: Forward and backward accumulation. *J. Atmos. Sci.* **52**: 2384–2403.

Dee DP, Uppala SM, Simmons AJ, Berrisford P, Poli P, Kobayashi S, Andrae U, Balmaseda MA, Balsamo G, Bauer P, Bechtold P, Beljaars ACM, van de Berg L, Bidlot J, Bormann N, Delsol C, Dragani R, Fuentes M, Geer AJ, Haimberger L, Healy SB, Hersbach H, Hólm EV, Isaksen L, Kållberg P, Köhler M, Matricardi M, McNally AP, Monge-Sanz BM, Morcrette J-J, Park B-K, Peubey C, de Rosnay P, Tavolato C, Thépaut J-N, Vitart F. 2011. The ERA-Interim reanalysis: Configuration and performance of the data assimilation system. *Q. J. R. Meteorol. Soc.* **137**: 553–597.

Dias J, Kiladis GN. 2014. Influence of the basic state zonal flow on convectively coupled equatorial waves. *Geophys. Res. Lett.* **41**: 6904–6913, doi: 10.1002/2014GL061476.

Gill AE. 1980. Some simple solutions for heat induced tropical circulations. *Q. J. R. Meteorol. Soc.* **106**: 447–462.

Hoskins BJ, Karoly DJ. 1981. The steady linear response of a spherical atmosphere to thermal and orographic forcing. *J. Atmos. Sci.* **38**: 1179–1196.

Hoskins BJ, Yang G-Y. 2000. The equatorial response to higher-latitude forcing. *J. Atmos. Sci.* **57**: 1197–1213.

Hoskins BJ, Yang G-Y. 2016. Energy change of equatorial waves when propagating in a zonally varying basic state. *J. Atmos. Sci.* **73**: 605–620.

Kiladis GN. 1998. Observations of Rossby waves linked to convection over the eastern tropical Pacific. *J. Atmos. Sci.* **55**: 321–339.

Lighthill J. 1978. *Waves in Fluids*. Cambridge University Press: Cambridge, UK.

Lin JL, Kiladis GN, Mapes BE, Weickmann KM, Sperber KR, Lin W, Wheeler M, Shubert SD, DelGenio A, Donner LJ, Emori S, Gueremy JF, Hourdain F, Rasch PJ, Roeckner E, Scinocca JF. 2006. Tropical intraseasonal variability in 14 IPCC AR4 climate models. Part I: Convective signals. *J. Clim.* **19**: 2665–2690.

Magaña V, Yanai M. 1995. Mixed Rossby-gravity waves triggered by lateral forcing. *J. Atmos. Sci.* **52**: 1473–1486.

Mak MK. 1969. Laterally driven stochastic motions in the Tropics. *J. Atmos. Sci.* **26**: 41–64.

Maruyama T, Tsuneoka Y. 1988. Anomalously short duration of the easterly wind phase of the QBO at 50 hPa in 1987 and its relationship to an El Niño event. *J. Meteorol. Soc. Jpn.* **66**: 629–634.

Matthews AJ, Kiladis GN. 1999. Interactions between ENSO, transient circulation, and tropical convection over the Pacific. *J. Clim.* **12**: 3062–3086.

Maury P, Lott F, Guez L, Duvel JP. 2013. Tropical variability and stratospheric equatorial waves in the IPSLCM5 model. *Clim. Dyn.* **40**: 2331–2344.

Ringer MA, Martin GM, Greeves CZ, Hinton TJ, James PM, Pope VD, Scaife AA, Stratton RA, Inness PM, Slingo JM, Yang G-Y. 2006. The physical properties of the atmosphere in the new Hadley Centre Global Environmental Model (HadGEM1). Part II: Aspects of variability and regional climate. *J. Clim* **19**: 1302–1326.

Tomas RA, Webster PJ. 1994. Horizontal and vertical structure of cross-equatorial wave propagation. *J. Atmos. Sci.* **51**: 1417–1430.

Wang B, Xie X. 1996. Low-frequency equatorial waves in vertically sheared zonal flow. Part I: Stable waves. *J. Atmos. Sci.* **53**: 449–467.

Webster PJ, Chang H-R. 1988. Equatorial energy accumulation and emanation regions: impacts of a zonally varying basic state. *J. Atmos. Sci.* **45**: 803–829.

Webster PJ, Holton JR. 1982. Cross-equatorial response to midlatitude forcing in a zonally varying basic state. *J. Atmos. Sci.* **39**: 722–733.

Wilson D, Mak M. 1984. Tropical response to lateral forcing with a latitudinally and zonally nonuniform basic state. *J. Atmos. Sci.* **41**: 1187–1201.

Yang G-Y, Hoskins BJ. 1996. Propagation of Rossby wave of nonzero frequency. *J. Atmos. Sci.* **53**: 2365–2378.

Yang G-Y, Hoskins BJ. 2013. ENSO impact on Kelvin waves and associated tropical convection. *J. Atmos. Sci.* **70**: 3513–3532.

Yang G-Y, Hoskins BJ, Slingo JM. 2003. Convectively coupled equatorial waves: a new methodology for identifying wave structures in observational data. *J. Atmos. Sci.* **60**: 1637–1654.

Yang G-Y, Hoskins BJ, Slingo JM. 2007a. Convectively coupled equatorial waves. Part I: Horizontal structure. *J. Atmos. Sci.* **64**: 3406–3423.

Yang G-Y, Hoskins BJ, Slingo JM. 2007b. Convectively coupled equatorial waves. Part II: Zonal propagation. *J. Atmos. Sci.* **64**: 3424–3437.

Yang G-Y, Hoskins BJ, Slingo JM. 2007c. Convectively coupled equatorial waves. Part III: Synthesis structures and extratropical forcing. *J. Atmos. Sci.* **64**: 3438–3451.

Yang G-Y, Slingo JM, Hoskins BJ. 2009. Convectively coupled equatorial waves in high resolution Hadley Centre climate models. *J. Clim* **22**: 1897–1919.

Yang GY, Hoskins BJ, Slingo JM. 2011. Equatorial waves in opposite QBO phases. *J. Atmos. Sci.* **68**: 839–862.

Yang GY, Hoskins BJ, Gray L. 2012. The influence of the QBO on the propagation of equatorial waves into the stratosphere. *J. Atmos. Sci.* **69**: 2959–2982.

Zhang C. 1993. Laterally forced equatorial perturbations in a linear model. Part II: Mobile forcing. *J. Atmos. Sci.* **50**: 807–821.